X-RAY SPECULAR REFLECTION STUDIES OF SILICON COATED BY ORGANIC MONOLAYERS (ALKYLSILOXANES).

I. M. Tidswell, B. M. Ocko, and P. S. Pershan
Division of Applied Sciences and Department of Physics
and S. R. Wasserman and G. M. Whitesides
Department of Chemistry
Harvard University
Cambridge MA 02138

and J. D. Axe
Department of Physics
Brookhaven National Laboratory
Upton NY 11973

Technical Report No. 21 (November 1989)

Interim Technical Report

(Accepted for publication in Phys. Rev. B)

PREPARED FOR DEFENSE ADVANCED RESEARCH PROJECTS AGENCY
1400 Wilson Boulevard
Arlington VA 22209

DEPARTMENT OF THE NAVY
Office of Naval Research, Code 1130P
800 North Quincy Street
Arlington VA 22217-5000

Project No.: a400011dd205
Contract No.: N00014-86-K-0756
Effective Date: 86 September 15
Expiration Date: 91 September 14

Principal Investigator: George M. Whitesides
(617) 495-9430

SECURITY CLASSIFICATION OF THIS PAGE

REPORT DOCUMENTATION PAGE

Form Approved
OMB No. 0704-0188

1a. REPORT SECURITY CLASSIFICATION Unclassified	1b. RESTRICTIVE MARKINGS
2a. SECURITY CLASSIFICATION AUTHORITY	3. DISTRIBUTION/AVAILABILITY OF REPORT Approved for public release; distribution unlimited
2b. DECLASSIFICATION/DOWNGRADING SCHEDULE	
4. PERFORMING ORGANIZATION REPORT NUMBER(S) Technical Report No. 21	5. MONITORING ORGANIZATION REPORT NUMBER(S)
6a. NAME OF PERFORMING ORGANIZATION Harvard University 6b. OFFICE SYMBOL (If applicable)	7a. NAME OF MONITORING ORGANIZATION DARPA
6c. ADDRESS (City, State, and ZIP Code) Office for Sponsored Research Holyoke Center, Fourth Floor Cambridge MA 02138-4993	7b. ADDRESS (City, State, and ZIP Code) 1400 Wilson Boulevard Arlington VA 22209-2308
8a. NAME OF FUNDING/SPONSORING ORGANIZATION ONR/DARPA 8b. OFFICE SYMBOL (If applicable)	9. PROCUREMENT INSTRUMENT IDENTIFICATION NUMBER
8c. ADDRESS (City, State, and ZIP Code) Chemistry Division, Code 1113 Office of Naval Research Arlington VA 22217-5000	10. SOURCE OF FUNDING NUMBERS PROGRAM ELEMENT NO. 86-K-0756 / PROJECT NO. / TASK NO. a400011dd2 / WORK UNIT ACCESSION NO.
11. TITLE (Include Security Classification) "X-ray Specular Reflection Studies of Silicon Coated by Organic Monolayers (Alkylsiloxanes)."	
12. PERSONAL AUTHOR(S) I. M. Tidswell, B.M. Ocko, P.S. Pershan, S.R. Wasserman, G.M.Whitesides and J.D.Axe	
13a. TYPE OF REPORT Technical 13b. TIME COVERED FROM _____ TO _____	14. DATE OF REPORT (Year, Month, Day) November 1989 15. PAGE COUNT
16. SUPPLEMENTARY NOTATION	
17. COSATI CODES FIELD / GROUP / SUB-GROUP	18. SUBJECT TERMS (Continue on reverse if necessary and identify by block number) x-ray specular reflectivity, silicon, alkylsiloxanes, structure, monolayer

19. ABSTRACT (Continue on reverse if necessary and identify by block number)

X-ray specular reflectivity is used to characterize the structure of silicon/silicon-oxide surfaces coated with chemisorbed hydrocarbon monolayer films (alkylsiloxanes). Using synchrotron radiation the reflectivity could be followed over 9 orders of magnitude, from grazing incidence to an incident angle $\theta \approx 6.5°$, or $q=(4\pi/\lambda)\sin(\theta)=0.8\text{Å}^{-1}$ allowing a spatial resolution of features approximately $\pi/0.8=4.0$Å along the surface normal. Analysis was performed by fitting the data to reflectivities

20. DISTRIBUTION/AVAILABILITY OF ABSTRACT ☐ UNCLASSIFIED/UNLIMITED ☒ SAME AS RPT. ☐ DTIC USERS	21. ABSTRACT SECURITY CLASSIFICATION Unclassified
22a. NAME OF RESPONSIBLE INDIVIDUAL Dr. Harold Guard	22b. TELEPHONE (Include Area Code) 202/696-4409 22c. OFFICE SYMBOL

DD Form 1473, JUN 86 *Previous editions are obsolete.* SECURITY CLASSIFICATION OF THIS PAGE

19. Abstract
"X-Ray Specular Reflection . . .," (Continued)

calculated from models of the surface electron density and by calculation of Patterson functions directly from the data. These procedures allow identification of an ≈17Å thick SiO_2 layer, a layer of head group region where the alkyl siloxane adsorbs to the SiO_2, and the hydrocarbon layer. The data also requires that the various interfaces have different widths. The fact that the same local hydrocarbon density of $0.85 g/cm^3$ is observed for both fully formed and partially formed monolayers with alkane chains of varying length excludes a model in which the partially formed monolayer is made up of separated islands of well formed monolayers. Measurements before and after chemical reaction of a monolayer in which the alkyl chain is terminated by an olefinic group demonstrates the ability to use x-ray reflectivity to characterize chemical changes. Effects of radiation damage on these types of measurements are described.

X-RAY SPECULAR REFLECTION STUDIES OF SILICON COATED BY ORGANIC MONOLAYERS (ALKYLSILOXANES).

I. M. Tidswell, B. M. Ocko†, and P. S. Pershan

Division of Applied Sciences and Department of Physics, Harvard University, Cambridge, Massachusetts, 02138

S. R. Wasserman and G. M. Whitesides

Department of Chemistry, Harvard University, Cambridge, Massachusetts, 02138

J. D. Axe

Department of Physics, Brookhaven National Laboratory, Upton, L.I., NY 11973

PACS Nos. 68.35.-p, 82.65.My, 82.80.Ej

† Present Address, Department of Physics, Brookhaven National Laboratory, Upton L.I., NY 11973

ABSTRACT

X-ray specular reflectivity is used to characterize the structure of silicon/silicon-oxide surfaces coated with chemisorbed hydrocarbon monolayer films (alkylsiloxanes). Using synchrotron radiation the reflectivity could be followed over 9 orders of magnitude, from grazing incidence to an incident angle $\theta \approx 6.5°$, or $q=(4\pi/\lambda)\sin(\theta)=0.8\text{Å}^{-1}$ allowing a spatial resolution of features approximately $\pi/0.8 \approx 4.0$Å along the surface normal. Analysis was performed by fitting the data to reflectivities calculated from models of the surface electron density and by calculation of Patterson functions directly from the data. These procedures allow identification of an ≈17Å thick SiO_2 layer, a layer of head group region where the alkyl siloxane adsorbs to the SiO_2, and the hydrocarbon layer. The data also requires that the various interfaces have different widths. The fact that the same local hydrocarbon density of 0.85g/cm^3 is observed for both fully formed and partially formed monolayers with alkane chains of varying length excludes a model in which the partially formed monolayer is made up of separated islands of well formed monolayers. Measurements before and after chemical reaction of a monolayer in which the alkyl chain is terminated by an olefinic group demonstrates the ability to use x-ray reflectivity to characterize chemical changes. Effects of radiation damage on these types of measurements are described.

INTRODUCTION.

Although Compton demonstrated the phenomena of small angle x-ray specular reflectivity by 1922,[1] we are not aware of any serious attempts to use the technique to characterize material surfaces before Parratt's measurements on copper surfaces in 1954.[2] Unfortunately his work was seriously limited by both the low brilliance (i.e.photons/[second-mm^2-mrad^2-0.1%$\Delta\lambda/\lambda$]) of the x-ray beams that were available at that time as well as the difficulty in obtaining a sufficiently smooth surface.[2] Improved surface preparation techniques and modern experimental methods have permitted study of a broad range of surfaces using conventional or rotating anode x-ray sources. Examples include studies of mercury and liquid metal surfaces,[3,4,5,6] of both coated and uncoated solid substrates,[7,8,9] and of surfactant monolayers on the surface of water.[10] The use of high brilliance synchrotron radiation by Als-Nielsen, Christensen, and Pershan to study specular reflectivity from the surface of the nematic liquid crystal 4-cyano-4'-n-octyloxybiphenol (8OCB) greatly enhanced the utility of x-ray specular reflection as a probe of interface and surface structure by increasing the range of accessible scattering angles.[11] Since then, a number of studies on surfaces of liquid crystals,[12,13,14,15,16] microemulsions,[17] simple liquids,[18, 19] insoluble monolayers on water[20,21,22] and metallic single crystals[23,24] have followed.

Most synthesis of organic monolayer films follows one of two different approaches. The first high quality monolayer films, produced by Blodgett and Langmuir, were made by dipping a substrate into a trough of water coated with a monolayer organic film on the surface.[25] Each pass of the substrate through the surface of the water applies a coat of either one or two

monolayers, depending on the specific structure of the monolayer. A second technique, forming generally more rugged monolayers, makes use of certain molecules which, in solution, spontaneously assemble to form uniform monolayer coatings on solid surfaces. A full review of the production, characterization and technological value of these and other types of organic thin films, together with extensive references to the literature, is given in the review by Swalen et al.[26]

In this paper we will describe measurements of x-ray reflectivity from silicon wafers coated with various alkylsiloxanes (i.e alkylsilanes, $R(CH_2)_nSiO_3$, covalently bonded to the silicon wafer surface by -oxygen-silicon bonds at the head of the chain with R being one of several moeities) using the technique of self assembly. Specular reflectivity from the air/hydrocarbon, hydrocarbon/silicon oxide, and the silicon oxide/crystalline silicon interfaces interfere to produce a combined reflectivity that is strongly dependent on the angle of incidence and the surface structure. Analysis of the measured angular dependence of the reflectivity allows a determination of the thickness of the hydrocarbon layer, the layer of silicon oxide between the hydrocarbon and the single crystal substrate, the widths of the interfaces between the various layers and the electron densities within each layer. Initial experiments were performed using a standard rotating anode x-ray generator. Higher quality data was obtained from the x-ray synchrotron radiation source at the National Synchrotron Light Source (NSLS).

Alkylsiloxane Coated Surfaces.

The present studies are concerned with monolayers that form spontaneously on the surface of silicon/silicon-oxide subtrates on

immersion of the sample in dilute anhydrous solutions of alkyl trichlorosilanes of the form $Cl_3Si\text{-}(CH_2)_n\text{-}X$, with n varying from 9 to 17. In the simplest case X is the methyl group ($-CH_3$), but we have also studied molecules in which the terminal groups were $-CH{=}CH_2$ and $-CHBr\text{-}CH_2Br$. We also measured the reflectivity of a monolayer prepared from a fluorocarbon of the structure $Cl_3Si\text{-}(CH_2)_2\text{-}(CF_2)_7\text{-}CF_3$. Although little experimental data exists on the formation of the alkylsiloxane film, it is assumed to proceed via the following steps[27]. On immersion of the silicon wafer into the trichlorosilane solution the silicon-chlorine bonds of the head group on the molecule are hydrolyzed by surface water on the substrate, replacing them with silanol groups (Si-OH). Loss of water results in chemical bonding of each silicon atom of the alkylsilyl moiety to the surface and to other alkylsilyl groups through covalent Si-O-Si bonds. The hydrocarbon film is therefore chemisorbed to the surface, in contrast to Langmuir-Blodgett films which are generally bound to the substrate through much weaker hydrogen bonds and Van der Waals interactions (physisorption). As a result alkylsiloxane monolayers are much more rugged and resistant to chemical attack than are Langmuir-Blodgett films.

Studies on alkylsiloxane monolayers, of the form $-Si\text{-}(CH_2)_n\text{-}CH_3$ with n = 12 to 20, that have been reported by Sagiv in a series of papers over the last decade[8,28,29,30,31] confirm their high stability and resistance to chemical attack.[32] The high contact angles that have been measured for all of these surfaces with water (110-115°) and hexadecane (38-45°) indicate that they have low surface energies and are not prone to contamination through physisorption of airborne hydrocarbons or water.[33] For comparison, clean silicon oxide surfaces, which are wet by water, have relatively high surface energy and readily adsorb airborne contaminants.

The alkyl groups in these systems are tightly packed. Ellipsometric measurements of well-formed monolayers are consistent with relatively dense packing and a mean thickness that equals (within experimental uncertainty)[34] the theoretical length of the fully extended alkane chain. This thickness could, however, also be consistent with a molecular tilt away from the surface normal by as much as 15°. Contact angle studies also support the interpretation of relatively dense well formed monolayers.[30] Both the chemical stability and the high surface uniformity make alkylsiloxane monolayers ideal for study.

The limited brilliance from the rotating anode x-ray source used in the previous study of the x-ray reflectivity from alkylsiloxane monolayers[8] restricted the range over which measurements could be taken to incident angles below 3° (corresponding to about $0.4Å^{-1}$). As a result, only the overall thickness of the adsorbed monolayer could be obtained with any confidence. The length measured was about 13% less than the length of a fully extended layer. This was explained in terms of an average area per molecule of $20Å^2$ and an associated tilt of each molecule of about 30° (e.g $\cos^{-1}(0.87) \approx 30°$). An unusually small width of 0.25Å was inferred for the alkyl/air and the silicon-oxide/alkyl interfaces, both being assigned the same width. Since this data was taken for a small range of incident angles, determination of small interface widths is very difficult, and we believe this estimate to be significantly too small. In the study reported here, the use of synchrotron radiation made it possible to measure the reflectivity out to incident angles of the order of 7°, allowing a more accurate determination of the interface widths.

REFLECTIVITY.

Even though the wavelength λ is comparable to atomic dimensions, and consequently comparable to the roughness of the surface, specular reflection of x-rays can be described by the Fresnel laws of classical optics.[19,35] The insert to Fig. 1 shows the kinematics for specular reflection of monochromatic x-rays from the surface of a solid. The refractive index of matter for x-rays of wavelength λ is given by $n = 1-\delta+i\beta$ where $\delta \approx \rho\lambda^2 r_o/2\pi$, ρ is the effective electron density, r_o the classical electron radius or the Thompson scattering length and $\beta \approx \lambda/4\pi\mu$ where μ is the x-ray absorption length. For the x-ray wavelengths of interest both δ and β are much less than one. The effective electron density ρ for low Z materials is just the total electron density of the material ρ_T. For materials where some fraction f of the electrons have binding energies that are greater than the incident x-ray energy, $\rho \approx \rho_T(1-f)$. Defining a critical angle $\phi_c \approx \sqrt{2\delta} = \lambda\sqrt{\rho r_o/\pi}$ and using the classical Maxwell's equations yields the expression for the Fresnel reflectivity (from a sharp interface) at small angles ϕ,[36]

$$R_F(\phi) \approx \left| \frac{\phi - (\phi^2 - \phi_c^2 + i\beta)^{1/2}}{\phi + (\phi^2 - \phi_c^2 + i\beta)^{1/2}} \right|^2 \qquad (1)$$

with ϕ defined as in the inset of Fig 1 and a critical angle $\phi_c = 0.222°$ for a silicon substrate and λ=1.5405Å radiation. Equation 1 can be re-expressed in terms of the scattering vector $q = (4\pi/\lambda)\sin(\phi)$ (Fig. 1) as

$$R_F(q) = \left| \frac{q - (q^2 - q_c^2 + 2i/\mu)^{1/2}}{q + (q^2 - q_c^2 + 2i/\mu)^{1/2}} \right|^2 \qquad (2)$$

$q_c = (4\pi/\lambda)\sin(\phi_c)$ is the "critical wavevector" in air and is independent of the wavelength: $q_c = 0.0316 Å^{-1}$ for silicon. This form for the reflectivity, shown for silicon as the solid line in Fig. 1, includes a slight rounding near the critical wavevector due to the small absorption factor. Away from $q \sim q_c$ absorption effects are negligible. For $q < q_c$ the radical is almost pure imaginary and the reflectivity is essentially 100% (i.e. total external reflection). Well above the critical angle the reflectivity is given by $R_F(q) \approx (q_c/2q)^4$.

For real surfaces the reflectivity can be expressed in terms of the average electron density[12,19,37],

$$R(q) = R_F(q)\left|\Phi(q)\right|^2 \qquad (3)$$

$$\Phi(q) = \int \frac{1}{\rho_\infty} \left\langle \frac{d\rho}{dz} \right\rangle e^{iqz} dz \qquad (4)$$

where $\left\langle \frac{d\rho}{dz} \right\rangle$ is the derivative of the electron density profile averaged over the in-plane coherence length of the x-rays and ρ_∞ is the electron density of the semi-infinite bulk. This form is valid for angles greater than approximately twice the critical angle, where refraction effects are negligible (i.e. when the Born approximation for the scattering is valid).

It is convenient to model the in-plane averaged electron density of a simple surface by a gaussian smeared step from $\rho=0$ to $\rho=\rho_\infty$:[12]

$$\langle \rho(z) \rangle = \frac{\rho_\infty}{2}\left(1 + \mathrm{erf}\left(\frac{z}{2\sigma}\right)\right) \qquad (5)$$

The average normal derivative is given by the Gaussian form

$$\left\langle \frac{d\rho}{dz} \right\rangle = \rho_\infty \frac{1}{\sqrt{2\pi\sigma^2}} e^{-z^2/2\sigma^2} \tag{6}$$

where σ, the root mean square average of the surface width, results from both the intrinsic width of the interface and the mean square average of the roughness of the surface.[19] The Fourier transform described by equation 4 yields

$$R(q) = R_F(q) e^{-\sigma^2 q^2} \tag{7}$$

an expression reminiscent of the Debye-Waller factor for solids. For $q \leq 0.4\text{Å}^{-1}$ the deviations between the measured reflectivity for the "bare silicon/silicon-oxide" wafer and the Fresnel reflection law in Fig. 1 are well described by a model surface of the form of equation 5 with an interface width of approximately 2.8Å. This model does not explain either the reflectivity of the uncoated silicon for $q > 0.4\text{Å}^{-1}$ nor the reflectivity from the alkylsiloxane coated samples that are also shown in Fig. 1. As implied above, since the reflectivity predicted by this model falls off with increasing incident angles as the product of a Gaussian and the $1/q^4$ term, the intensity becomes the limiting factor in measuring the reflectivity at larger angles.

The simplest physically reasonable model for the surface of the siloxane coated surface consists of a silicon substrate with electron density ρ_{Si} that is covered uniformly with a hydrocarbon layer of length L and electron density ρ_{CH}. If the silicon/alkane and alkane/air interfaces have widths σ_1 and σ_2 respectively the normal derivative is of the form:

$$\left\langle \frac{d\rho}{dz} \right\rangle = (\rho_{Si} - \rho_{CH}) \frac{1}{\left(2\pi\sigma_1^2\right)^{1/2}} e^{-z^2/2\sigma_1^2} + \rho_{CH} \frac{1}{\left(2\pi\sigma_2^2\right)^{1/2}} e^{-(z-L)^2/2\sigma_2^2} \quad (8)$$

Application of equations 3 and 4 to equation 8 generates

$$\frac{R(q)}{R_F(q)} = \left|\Phi(q)\right|^2 = \left| \frac{(\rho_{Si}-\rho_{CH})}{\rho_{Si}} e^{-q^2\sigma_1^2/2} + \frac{\rho_{CH}}{\rho_{Si}} e^{-q^2\sigma_2^2/2} e^{-iqL} \right|^2 \quad (9)$$

For small angles, such that $q\sigma_{1,2} << 1$, this expression simplifies to the form

$$\frac{R(q)}{R_F(q)} \approx \left(\frac{\rho_{Si}-\rho_{CH}}{\rho_{Si}}\right)^2 + \left(\frac{\rho_{CH}}{\rho_{Si}}\right)^2 + 2\left(\frac{\rho_{Si}-\rho_{CH}}{\rho_{Si}}\right)\left(\frac{\rho_{CH}}{\rho_{Si}}\right)\cos(qL) \quad (10)$$

Since $(\rho_{Si}-\rho_{CH})/\rho_{Si} \approx \rho_{CH}/\rho_{Si}$ this model predicts the observed minimum in the reflectivity (Fig. 1) when $q = (4\pi/\lambda)\sin(\phi) = \pi/L$ where L is approximately equal to the thickness of hydrocarbon film.

A more general model, with N separate layers, has the form

$$\left\langle \frac{d\rho}{dz} \right\rangle = \sum_0^N (\rho_i - \rho_{i+1}) \frac{1}{\left(2\pi\sigma_{i+1}^2\right)^{1/2}} e^{-(z-D_i)^2/2\sigma_{i+1}^2} \quad (11)$$

where ρ_0 corresponds to the electron density of the substrate (ρ_∞ of Eq. 5), which in the present example is crystalline silicon, $\rho_{N+1} \approx 0$ is the density in air, L_i is the thickness of the i^{th} layer and $D_i = \sum_{j=1}^{i} L_j$ is the distance from the crystalline silicon surface to the interface between the i^{th} and the $(i+1)^{st}$ layers (i.e. $D_0 = 0$). The Fourier transform for this form yields

$$\frac{R(q)}{R_F(q)} = \left|\Phi(q)\right|^2 = \left| \sum_0^N \left(\frac{\rho_i - \rho_{i+1}}{\rho_0}\right) e^{-iqD_i} e^{-q^2\sigma_{i+1}^2/2} \right|^2 \quad (12)$$

where $\rho_o = \rho_{Si}$ is the density of crystalline silicon, We will show below that the data for the alkylsiloxane coated silicon wafers shown in Fig. 1 are well described by a model in which N=3.

The coherence length for the x-rays is a function of the spectrometer resolution, being a function of the slit widths and x-ray path lengths. Typically the coherence length *in the plane of the surface* is also a function of the inverse incident angle. At the rotating anode, this length is of order $4x10^4$Å at the critical angle and $3x10^3$Å at 3°. The corresponding lengths at the synchrotron are about 10^5Å and $8x10^3$Å. At these angles, the region of the sample illuminated is about 6mm normal to the plane of incidence by 5-20mm within the plane of incidence, depending on the precise slit widths.

Surfaces that are inhomogeneous in the plane of the surface give rise to non-specular surface diffuse scattering (SDS). Although SDS has been observed by us and others[19,38,39], for the silicon substrates used in this study the surface diffuse scattering, integrated over the spectrometer resolution at $q \approx 0.04$Å^{-1} was less than $\approx 10^{-2}$ of the intensity of the specular reflection and we have not carried out systematic measurements of surface diffuse scattering from these samples.

EXPERIMENTAL DETAILS

Preparation of Samples.[34]

Sample substrates were made from highly polished silicon (100) wafers obtained from Semiconductor Processing Corp. of Boston Mass. Each sample consisted of a 1" strip cut from a 3" diameter wafer that was either 0.08", 0.125" or 0.200" thick. The thinnest 0.08" wafers were found to be warped with typical surface normal variations of about 0.05° over the central 5cm of the wafer, compared to 0.005° for the same region of the

thicker wafers. Although early studies and some of the synchrotron data were taken on the thin substrates, most of the data reported were carried out on the 0.125" wafers.

The silicon wafers were cleaned by immersing in a H_2O_2/sulfuric acid mixture (70:30 v/v concentrated H_2SO_4, 30% H_2O_2 at 80°C for one hour). This strongly oxidizing combination removes all organic contaminants on the surface but does not disturb the native silicon oxide layer. The wafers were then rinsed and stored under distilled water before use. Prior to preparing the monolayers, the wafers were removed from the water and blown dry under a stream of argon. Decyl-, undecyl-, dodecyl-, tetradecyl-, hexadecyl- and octadecyltrichlorosilane (i.e. $Cl_3Si\text{-}(CH_2)_n\text{-}CH_3$ with n = 9, 10, 11, 13, 15, 17 respectively) were used to form the alkane monolayers.

After rinsing in distilled water, each wafer was allowed to react with a solution of alkyl trichlorosilane (≈1%, w/w in hexadecane) for up to 30 minutes, before being removed from the solution and rinsed with hexane and ethanol. These operations were performed under a dry, inert atmosphere when conditions of high ambient humidity existed. The samples were autophobic to solution on removal from the solution of alkyl trichlorosilane.

The following procedure was followed to minimize surface contamination. Ellipsometric measurements of the monolayer thicknesses were made within 5 minutes of removal of the sample from water.[34] Coated wafers were typically then stored in air for periods as long a one week before x-ray measurements were made. No change was noted in the x-ray data between measurements of fresh samples and of samples stored for up to one month after preparation. Immediately prior to taking the x-ray data, samples were rinsed with dry ethanol to remove organic contamination,

blown dry with dry nitrogen and immediately transferred to the x-ray spectrometer. X-ray photoelectron spectroscopy (XPS) data for the samples were taken some time (generally about two months) after the x-ray measurement.

Partially complete monolayers were formed by removing the sample from the solution in a time shorter than that required for a full film to form.[40] Ellipsometric measurements were used to obtain one estimate of the degree of coverage.[34] The alkene terminated film was made by the same method as for the alkane films, but starting with a trichlorosilane with the appropriate alkene tail, namely $Cl_3Si\text{-}(CH_2)_{15}\text{-}CH{=}CH_2$. The brominated sample was made from one of the alkene terminated samples, after the initial x-ray reflection measurement was completed, by immersing the sample in a 2% by volume solution of elemental bromine in methyl chloride. The fluorocarbon sample was formed in a similar manner to the alkylsiloxane monolayers, again using the relevant precursor ($Cl_3Si\text{-}(CH_2)_2\text{-}(CF_2)_7\text{-}CF_3$). The use of this form was necessitated by chemical restrictions which make the much simpler fluorosilane molecule $Cl_3Si\text{-}(CF_2)_9\text{-}CF_3$ difficult to synthesize. Further details of the sample preparations are given in other papers.[34,40]

X-Ray Technique.

Most of the data reported here were taken on beam line X-22B at the NSLS facility at Brookhaven National Laboratory. Some of the low angle data were taken on the rotating anode x-ray generator of the Harvard Materials Research Laboratory in order to locate the position of the lowest-order destructive interference minima and make preliminary judgments of sample quality.

The rotating anode measurements were made using the configuration shown in Fig. 2a. The monochromator was either a single- or triple-bounce germanium (111) crystal [Ge(111)] set to accept copper $K\alpha_1$ radiation (wavelength 1.5405Å). At small incident angles ϕ, the intersection of a collimated beam of width w covers a length $\sim w/\sin(\phi) >> w$, with the size of the beam incident on the sample being defined by slit S_2 and some preliminary collimation provided by slit S_1. For angles below $\approx 1°$ the dimensions of S_2 were approximately 100μm horizontal width by 6mm, and 500μm x 6mm for larger angles, with similar dimensions for S_1. These slit dimensions were chosen to satisfy the conditions of: 1) all the beam being incident on the central 50mm of the sample, 2) to avoid detector saturation and 3) to maximizing the incident flux at large incident angles. The principal purpose of slit S_3 was to reduced the background scattering by trimming the tails of the slit scattering from S_2. S_3 was closed symmetrically to the point that it had a measurable effect on the count rate and was then opened slightly. S_4 was opened to dimensions of approximately 1mm x 10mm assuring that all the beam reflected off the sample was detected. The monitor and detector were NaI(Tl) scintillation counters, the monitor being placed at 90° to the beam with a small piece of plastic scattering approximately 0.03% of the beam into the detector. A reflection intensity dynamic range of about 10^7 was achieved for a typical series of scans lasting approximately 12 hours.

At the synchrotron a wavelength of 1.7096Å was used, the experimental configuration being shown in fig 2b. A single bounce Ge(111) crystal was used. Slit S_1 actually consisted of two slits about 50mm apart: the first was a triangular slit used to coarsely define the useful part of the beam in the horizontal direction, the second section defining the vertical

definition of the beam. Although these slits were crudely set, they significantly reduced the background scattering inside the experimental hutch. S_2 was the beam defining slit, with slit S_3 trimming the tails of the slit scattering but not affecting the counts in the main beam. As a result of the very long distance from the source to the spectrometer no further collimation of the beam was necessary. The slit widths were similar to those used at Harvard, except that at the largest angles a beam width of 1mm was used. Because of the very intense beam, at very small angles (below 1°) the detector was placed at 90° to the beam with a small sheet of plastic scattering about 0.03% of the beam into the detector. The detector was switched to a direct position at about 0.8°. S_3 was opened to 1mm at an angle of about 3°. Slit S_4 was opened to cut down the direct scattering from sources other than the sample and S_5 was therefore set wide enough to accept all the specular beam reflected from the sample. All data were normalized to the counts recorded in a beam monitor located between the beam defining slit S_2 and the trimming slit S_3. It consisted of a second plastic sheet that scattered about 0.02% of the direct beam into a second scintillation detector at 90° to the direct beam. A reflected intensity dynamic range of 10^9 was obtained over the period of about four hours necessary to record a typical set of scans for one sample.

For both experimental configurations samples were aligned by using the diffractometer in a non-dispersive three-crystal mode in which a single- or triple-bounce Ge(111) analyzer crystal was placed between the last slit and the detector. With the sample removed the analyzer was in a dispersive orientation; nevertheless a good measure of the incident angle for the direct beam was obtained by rotating the analyzer crystal to maximize the signal in the detector. In order to obtain an approximate

alignment the sample was then translated into the beam and, by an iterative process in which ϕ was rotated and the sample translated, the sample was aligned parallel to, and obscuring half of the beam. Next the sample was rotated to an angle just below the critical angle (typically 0.15°) and the detector was scanned through the specular reflection (i.e a 2θ scan) in order to check the alignment and figure error of the sample. Since the initial alignment procedure was prone to errors arising from macroscopic substrate warpage (typically from the edges from which no scattering is measured) the final sample alignment was obtained by setting ϕ equal to half of 2θ. The analyzer crystal was then removed leaving the detector centered on the specularly reflected beam. Finally the sample was translated through the beam parallel to the surface normal in order to ensure that the incident beam was correctly centered on the sample.

Although the angular dependence of the specular reflectivity was measured by a series of "ϕ-2θ" scans in which ϕ is continually maintained equal to half of 2θ the alignment was frequently checked by performing 2θ scans at fixed ϕ. This procedure ensured accurate sample alignment to within 0.01° and was also a check that the figure error of a sample was acceptable. In order to correct for the fact that the signal observed when the spectrometer is set to the specular condition consists of the sum of the specular reflection and diffuse scattering, "background scattering" ϕ-2θ scans were taken with 2θ offset from the specular condition by $(2\theta)=2\phi\pm 0.3°$. For each incident angle the specular reflectivity was identified as the difference between the three appropriately normalized ϕ-2θ scans: i.e. specular reflection = $I(\phi,2\theta) - \frac{1}{2}[I(\phi,2\theta-0.3°) + I(\phi,2\theta+0.3°)]$. Point-by-point background subtraction was required since the diffuse scattering depended on the incident angle. The background for three different angles of

incidence are illustrated for data taken at NSLS in Fig. 3 by ϕ-scans at fixed 2θ. The signal reported as the specular reflectivity is obtained by subtracting the background count rate from the peak count rate, as described.

Although the experiments were carried out with the samples contained in a sealed cell that was filled with air or helium, the results discussed below demonstrated that airborne hydrocarbons were not fully eliminated from the helium-filled cell. The x-rays were incident through Kapton windows, with an angular access of up to 7° and approximately 75% transmissivity.

RESULTS

Alkylsiloxanes with C_{10}, C_{12}, and C_{18} alkyl chains

Data

Fig. 1 shows the results of synchrotron measurements of the reflectivity R(q) (after background subtraction) for alkylsiloxane monolayers of differing length and for the uncoated silicon. This figure also shows the Fresnel reflectivity for an ideal step surface of a material with the bulk density of silicon. Without any sophisticated analysis, there are a number of prominent features that can be immediately interpreted. All of the alkylsiloxane-covered samples exhibit spectroscopic structure, most notably a sharp minimum at a scattering vector of between 0.1 and 0.25Å^{-1}, and other minima and maxima at larger q. Independent rotating anode data (not shown here) have confirmed the position of the first minimum and the general form of the reflectivity at wavevectors below about 0.4Å^{-1}.

We interpret the first minimum as the result of destructive interference between reflections from the front and back surfaces of the alkane layer of thickness L. For thin enough films, or for films in which the electron density is not too high, the position of the minimum in this interpretation is given by the condition that $qL=\pi$ or $\phi=\sin^{-1}(\lambda/4L)$. For either thicker or denser films, refraction effects are, however, important and the destructive interference occurs for $q'L = L\sqrt{q^2-q_c^2} =\pi$. For a fully-formed hydrocarbon layer of the type of interest here, $q_c \approx 0.021 Å^{-1}$ would be the critical wavevector of a semi-infinite sample with the same electron density as the hydrocarbon layer. The positions of the minima for the C_{10}, C_{12} and C_{18} correspond to $q=0.21 Å^{-1}$, $0.19 Å^{-1}$ and $0.13 Å^{-1}$ respectively. Taking the refraction correction into account, the thicknesses of the C_{10}, C_{12} and C_{18} alkane layers, for this interpretation of the position of minima, corresponds to 14.4Å, 16.3Å and 23.6Å respectively. The best straight line that can be drawn through these points (i.e. $L = 1.16\times n +2.56$ Å) yields corresponding values 14.1Å, 16.5Å and 23.4Å. This expression for L should be compared with the published expression $L= 1.265\times n + 1.5$ Å, which gives 14.2Å,16.7Å and 24.3Å for the maximum extension of an aliphatic chain $-(CH_2)_{n-1}CH_3$ with n = 10, 12 and 18 respectively.[41] A more detailed model of the surface, in which the thickness of the silicon head group can be separated from that of the hydrocarbon chain, will be described below. This model gives values for L that are somewhat shorter than the results quoted here.

A similarity of the reflectivities from these three samples is that they all fall below the Fresnel curve. This indicates that the reflecting interfaces are not ideally sharp, but have some associated widths. From the fact that the reflectivities are all about 10^{-1} to 10^{-3} of the Fresnel

reflectivity at $q \approx 0.7\text{Å}^{-1}$ to 0.8Å^{-1}, the interface widths of all of these samples, as determined by the mean fall off of the reflectivity curve at increasing angles, is between 2.5 and 5.5Å.

The deep nature of the minima (cancellation of between 10^{-2} and 10^{-3}) indicates that at the angle of the minimum, the amplitude of the wave reflected from the top and bottom interfaces of the hydrocarbon chain are of almost equal magnitude. This deep cancellation implies that the electron density of the hydrocarbon layer is very close to being half that of the silicon substrate. This conclusion is reasonably consistent with the known value of approximately 0.38 for the ratio of the electron density of bulk hydrocarbon to that of silicon.

More accurately, one must also consider the widths of the two interfaces, specifically the differences in the widths between the two interfaces. With increasing angle the amplitude of the reflectivity signal due to the rougher of the two interfaces will fall off faster than that from the smoother. Since the depth of the minimum depends on the relative amplitudes of the reflectivities from the two interfaces at the value of q where they are out of phase by π, the relative widths of the interfaces can have a dramatic effect on the depth of the dip in the reflectivity. For the alkylsiloxane monolayers the cancellation of the dip is actually more complete than would be expected for chain packed with a bulk liquid hydrocarbon density if interface widths were neglected. The discrepancy has its origin in either the density of the hydrocarbon layer being considerably higher than the bulk liquid, or the width of the internal interface being greater than the external interface. More detailed modeling is used to address this question later.

Closer examination of the reflectivity reveals that minima at larger angles do not occur at positions that are integral multiples of the positions of the smallest angle minimum. This suggests the presence of other surface structure with a different length scale from that of the hydrocarbon layer. It is difficult to extract this additional length from a qualitative analysis since the different widths of the interfaces can shift the positions of the minima. A more detailed analysis of these length scales will also follow.

Evidence of an experimental problem with surface contamination of the uncoated silicon sample during the x-ray measurements can be seen in the data in Fig. 1. At large scattering vectors alternate points were measured in scans taken approximately 60 minutes apart, and as can be seen the points from the two different scans are offset from one another. We believe this is due to the continuous build up of a contamination layer on the sample. At the time of the measurement this layer was probably about 5Å thick, however the progressive shifting of the minimum to lower angles in data taken a few hours later confirmed the build up of contaminants on the surface. Some of the contamination is probably caused by the presence of hydrocarbons in the helium flowing through the sample cell during the experiment since there was a significantly slower build up on samples left exposed to air for a similar length of time. No such problem was observed with the lower energy alkylsiloxane coated surfaces

Analysis.

Detailed analysis of the alkylsiloxane surface electron density was carried out by least-squares fitting of the data to a version of the N layer

model for $\Phi(q)$ that was corrected for the effects of refraction. The correction involved replacing the $\{qD_i\}$ in the factor

$$\left\{e^{-iqD_i} e^{-q^2\sigma_{i+1}^2/2}\right\}$$

of equation 12 by

$$qD_i = \sum_{j=1}^{i} q_j L_j \qquad (13)$$

where $q_j = (q^2 - q_{cj}^2)^{1/2}$ and q_{cj} is the critical wavevector for the j^{th} layer. In principle a similar correction is required for the Gaussian term. The corrections are, however, small, and were neglected.

Fig. 4 shows the data for the C18 coated silicon wafer, in the form of $R(q)/R_F(q)$. The solid lines display a set of fits for models with 1, 2, and 3 layers respectively, i.e. N = 1,2 and 3 in equation 12. The parameters of these fits are given in the columns labeled N=1,2 and $3^{(+)}$ in Table I. Since the N=1 and 2 models are obviously inadequate, these fits were done using only a subset of the data, the width of the alkane/air interface being constrained to follow the observed average fall off in the reflectivity at large q. In addition, for the N=2 model the fitting algorithm was unable to fix either the width of the silicon/silicon oxide interface ($\sigma_{0,1}$) or the thickness of the silicon oxide layer (L_1) and the values of these parameters appearing in Table I for N=2 were chosen such that the maxima and minima in the model were at approximately the same positions as in the data, and the depth of the second minimum was also approximately correct. Given the obvious inadequacies of the 1 and 2 layer models, confidence limits for the parameters of these models are not particularly meaningful.

The motivation for the second layer comes from the well-known fact that on exposure to O_2, crystalline silicon forms a relatively stable oxide layer that is about 10-20Å thick.[42] In addition, it is difficult to see how a

hydrocarbon layer on its own could give rise to the non-integral positions of the high angle minima. A more compelling case specific to the present data are the results for the Patterson function (Fig. 5)

$$Z(s) \equiv \frac{1}{2\pi}\int_{-\infty}^{\infty} dq|\Phi(q)|^2 e^{-iqs} = \frac{1}{\rho_\infty^2}\int_{-\infty}^{\infty} \left\langle \frac{d\rho(z)}{dz} \right\rangle \left\langle \frac{d\rho(s+z)}{dz} \right\rangle dz \qquad (14)$$

calculated from the data for $R(q)/R_F(q) = |\Phi(q)|^2$ in Fig. 4. The dashed line in Fig. 5 was calculated directly from the data by correcting the critical angle to correspond to that inside the bulk, assuming $|\Phi(q)|^2 = |\Phi(-q)|^2$ and using a smooth Gaussian to extrapolate from the last measured point at $q \approx 0.8\text{Å}^{-1}$ to the vanishing of $|\Phi(q)|^2$ at $q = \pm 8\text{Å}^{-1}$, well beyond the measured range, where the reflectivity is essentially zero. For the C18 alkylsiloxane this Gaussian corresponded to a surface having a 3.6Å interfacial width. The peak at $s \approx 40$Å in Fig. 5 indicates that in addition to the main hydrocarbon layer of approximately 20Å thickness, there is a second layer, also of about 20Å thickness, with an interface that is either 20Å above the alkane/air interface and 40Å above the silicon-oxide/alkane interface, or 20Å below the silicon-oxide/alkane interface and 40Å below the alkane/air interface. While the former suggestion is unphysical, the latter could correspond to the native silicon oxide layer, the silicon/silicon oxide interface convoluted with the hydrocarbon/air interface being responsible for the peak at about 40Å. The fit of the $R/R_F(q)$ data gave the values of the parameters in Table I for the N=2 model with the electron density $\rho_1 = 0.968$ and a layer thickness $L_1 = 17.4$Å being just what is expected for the silicon-oxide layer.

The one uncertainty associated with a Patterson function (in addition to any systematic errors introduced by the wavevector correction and the

interpolation of points) is whether or not the structure could be an artifact associated with the way the data are extrapolated past the last measured point.[43] The solid line indicates the result that is obtained from multiplying the data by a Gaussian with $\sigma_p = 0.3\text{Å}^{-1}$ such that the data for q greater than 0.8Å^{-1} make no important contribution to the integral: i.e. $\exp(-(0.8/0.3)^2/2) \approx 3\times10^{-4}$. As illustrated by Eq. 15 the Patterson function calculated this way can be interpreted as the convolution of a Gaussian resolution function with the Patterson function Z(s) of Eq. 14:

$$Z_G(s) \equiv \frac{1}{2\pi}\int_{-\infty}^{\infty} dq |\Phi(q)|^2 e^{-q^2/2\sigma_p^2} e^{-iqs}$$

$$= \frac{1}{\rho_\infty^2}\int_{-\infty}^{\infty}\left(\int_{-\infty}^{\infty}\left\langle\frac{d\rho(z)}{dz}\right\rangle\left\langle\frac{d\rho(s+s'+z)}{dz}\right\rangle dz\right)\frac{1}{\left(2\pi\sigma_p^2\right)^{1/2}} e^{[-(s')^2\sigma_p^2/2]} ds'$$

$$= \int_{-\infty}^{\infty} Z(s+s')\frac{1}{\left(2\pi\sigma_p^2\right)^{1/2}} e^{[-(s')^2\sigma_p^2/2]} ds' \qquad (15)$$

This procedure is equivalent to viewing the auto correlation function through a "real-space Gaussian filter" which reduces the amplitudes of the peaks and increase their widths. Since the structure at $s \approx 40\text{Å}$ is still present (albeit smeared out) it can not be attributed to a "truncation artifact."

Unfortunately the N=2 model is not able to describe the reflectivity data at large q and the $N=3^{(+)}$ that was used to construct the solid line in Fig. 4c is obtained by adding a third layer in the immediate vicinity of the

silicon/silicon-oxide interface. The reduced χ^2 for this fit, using the 95 data points above 0.1Å^{-1} is approximately 80 when weighted by Poisson statistics, as compared to a χ^2 of approximately 800 for the two layer fit and 2000 for the one layer fit for the same points. While this large χ^2 does indicate some systematic errors, it is quite clear that this model explains all of the main features of the data very well. The main differences between the electron densities of the N=3$^{(+)}$ model and the N=2 model occur at the silicon oxide/hydrocarbon interface, with the properties of the other interfaces remaining essentially unchanged. In contrast to the N=2 model, for the N=3$^{(+)}$ model the fitting algorithm was able to determine the thickness of the silicon oxide layer. The width of the silicon/silicon oxide interface could, however, still not be determined from the existing data set. In fact the minimum value of χ^2 is obtained for an infinitesmally small value for the width of this interface. The fits were carried out with σ_{01} arbitrarily set equal to 1Å, the other parameters being relatively independent of the precise value. Similarly, since the data were only taken to $q \leq 0.8$Å^{-1}, the results for the fine structure of the silicon oxide/alkane interface are not unique. The solid line in Fig 4c is the best fit for the N=3$^{(+)}$ model when $\rho_2 > \rho_0$. The confidence limits listed in Table I for these parameters, as well as the possible variations in the model (i.e. uniqueness) for the silicon oxide/alkane interface, will be discussed below.

Fig. 6a, b and c display the electron density as a function of distance from the surface for the N=1,2 and 3$^{(+)}$ models used to calculate the $R(q)/R_F(q)$ in Fig 4. Fig. 6d illustrates that there are only small quantitative differences between the electron densities for the three models by superposing the three offset curves in Fig. 6a, b and c. The differences in the real-space electron densities are also illustrated by the Patterson

functions calculated from the same N=1,2 and $3^{(+)}$ models and displayed in Fig. 7. While the extra structure at z≈40Å constitutes a significant difference between the N=1 and the other models, the differences between the N=2 and $N=3^{(+)}$ models are relatively subtle, consisting principally of the shoulder at s≈30Å. The main reason for the discrepancies at small length scales between the $\langle\partial\rho(z)/\partial z\rangle\langle\partial\rho(0)/\partial z\rangle$ calculated from the data and from the models is that in the absence of measured reflectivities for $q\geq 0.8\text{Å}^{-1}$ the data was extrapolated by a Gaussian, artificially extending the range of the data but terminating any oscillation *which might be present* if measured. This termination, which could well apply an incorrect roughness, also implies an artificial amplitude to the value of the Patterson function at small s. Although this uncertainty does not affect the peak at $q\approx 40\text{Å}^{-1}$, it does minimize the value of quantitative comparisons between the Patterson functions calculated from the data and from the models at small s.

In order to assess the confidence limits for the $N=3^{(+)}$ parameters, a set of fits were carried out in which the electron density associated with the interface, ρ_2, was constrained to different values and all other parameters in the model, except for the width of the silicon/silicon-oxide interface σ_{01}, were allowed to vary. Since most of the parameters are tightly coupled, this procedure is necessary to estimate the range of the density ρ_2 allowed by the data with this model. Fig. 8b,c displays the results for what we subjectively consider to be values of ρ_2 surrounding the local minimum in χ^2 at $\rho_2\approx 1.25$ that yield borderline acceptable reflectivity fits. These correspond to values of χ^2 that are approximately 25% larger than the minimum. The $N=3^{(+)}$ fit that generated the minimum χ^2, Fig. 4c is shown again for comparison in fig. 8a. The parameters obtained from these fits are listed in Table I as

$N=3^{(+1)}$ and $3^{(+2)}$. Similarly the confidence limits in Table I are arbitrarily set at the values that increase χ^2 by approximately 25%, the fits being completed by the same procedure as used to obtain fig. 8b and c.

In order to illustrate the significance of these variations, the real-space electron density for all the three $N=3^{(+)}$ models are displayed in Fig. 9a,b,c with all of the interface widths set to be zero, and in Fig. 9e,f,g with the appropriate interface widths. Note that the very high peak density that appears for the second layer in the $3^{(+1)}$ column is misleading since this layer is also very thin. The widths of the two interfaces for this layer are similar and this similarity has the effect of producing two smeared steps in $d\rho/dz$, of opposite signs, which almost exactly cancel to give the profile shown in Fig. 9f. Also, the sharp feature in Fig 9g could be smeared out with no appreciable change to the fit quality. Figs. 9f and 9g therefore give one indication of the confidence limits that we believe can be assigned to the structure based on the local minimum in χ^2 surrounding the value of $\rho_2 \approx 1.25$. In addition there is a second local minimum surrounding the value of $\rho_2 \approx 0.82$. The best fit parameters for this minimum are listed in Table I in the column $3^{(-)}$ and the results for the $R(q)/R_F(q)$ are illustrated in Fig. 8d. In this case the minimum value of χ^2 is about 78 when calculated using the same data as previously.

Table I: Parameters for fits of the N=1,2,and 3 layer model described by Eq. 12 to the data for the C18 alkylsiloxane-coated silicon wafer. The results calculated from the columns N=1,2 and N=$3^{(+)}$ are shown in Fig. 4. The model reflectivities for parameters $3^{(+)}$, $3^{(+1)}$, $3^{(+2)}$ and $3^{(-)}$ are illustrated in Fig. 8a, b, c and d respectively and the real-space densities are illustrated in Fig. 9. The sixth line gives the lengths as measured by the graphical technique described in the text.

Layer		N=1	N=2	$3^{(+)}$	$3^{(+1)}$	$3^{(+2)}$	$3^{(-)}$
Layer thickness L_j(Å)							
SiO_2	L_1 (Å)	-	17.4*	16.8±0.9	17.5	16.7	12.7±1.5
Interface	L_2 (Å)	-	-	0.7±0.6	0.014	0.8	7.0±1.5
-(CH_2)-	L_3 (Å)	23.7	23.0	23.5±0.3	23.4	23.5	21.3±0.5
-(CH_2)- graph	L_3 (Å)	20.8	20.4	21.4±0.5	21.2	21.6	21.2±0.5
	ρ_j/ρ_o						
SiO	ρ_1/ρ_o	-	0.968	0.96±0.01	0.96	0.96	0.96±0.01
Interface	ρ_2/ρ_o	-	-	$1.25^{+20}_{-0.1}$	20*	1.12*	0.82±0.15
-(CH_2)-	ρ_3/ρ_o	0.45*	0.42	$0.43^{+0.05}_{-0.02}$	0.46	0.43	$0.43^{+0.06}_{-0.02}$
	$\sigma_{i,j}$ (Å)						
Si/SiO_2	σ_{01} (Å)	-	1.0*	1.0*<2.0	1*	1*	1*<2.0
SiO_2/Int.	σ_{12} (Å)	-	-	1.0*<3.0	2.39	0	1*<2.0
Int/(CH_2)	σ_{23} (Å)	4.9	4.2	3.2±0.5	2.44	3.4	2.4±0.8
(CH_2)/Air	σ_{34} (Å)	2.6*	2.3*	2.4±0.3	2.6	2.3	2.4±0.4

* Parameter held constant during fit.

Although some of the N=3(+) and 3(-) parameters are quite different, the real-space densities, as illustrated in Fig. 9e and 9h, and superposed in Fig. 9i, have only small quantitative differences only in the region of the SiO_2/alkane interface. In fact, for all of the models described in Table I (i.e. as shown in Figs. 6d and 9) the small, quantitative differences between the electron densities are much less significant than would appear from the parameters in the Table.

That different sets of parameters give rise to similar electron density profiles suggests that the parameters themselves are not the most meaningful way to interpret the reflectivity data. In the present case, the N=3 models were introduced because the reflectivity data clearly indicated that the SiO_2/hydrocarbon interface had some structure. However, since the various model electron densities resultant from these different sets of parameters are similar, the procedure used does allow a relatively unambiguous determination of the electron density responsible for the observed specular reflection. Furthermore, the solid lines in Fig. 6 illustrate how these electron densities can be interpreted to obtain a relatively precise, model independent, value for the thickness of the hydrocarbon region.

We expect that the dominant effect giving rise to the observed interfacial widths is the roughness of the outer SiO_2 surface. If this substrate roughness is coated by a fixed thickness of hydrocarbon then the thickness can be inferred from the distance between adjacent maxima in the second derivative of the density $d^2\rho/dz^2$. The solid construction lines in Fig. 6 illustrate a graphical procedure for locating these points. The results obtained on applying this technique to the models in Fig. 6 and 9 are listed in Table I in the row -(CH_2)-graph. Although there is some variation

between the N=1,2 and 3 models (the N=1 and 2 models in any case being poor fits to the reflectivity profile), the results for the various N=3 models are, within errors, identical. While this technique is somewhat arbitrary, we believe it gives a reasonable estimate of the length of the hydrocarbon chain *excluding* the silicon head group. The mean value of 21.3±0.4Å is shorter than the length obtained from the position of the dip (23.6Å) (dashed arrow in Fig. 6) due to the specific exclusion of the head group from the graphical length determination.

Since the $N=3^{(+)}$ and $3^{(-)}$ models give essentially the same structure, we will continue the analysis of the other samples in terms of the model that gives the best fit for that specific sample (holding some parameters fixed if necessary to obtain a physically reasonable structure. This is necessary for those parameters with large uncertainties).

Further insight into the physical significance of the electron densities obtained from the N=3 model can be obtained by consideration of fits shown in Fig. 10 a and b, for the C10 and C12 respectively, coated wafers that are analogous to those shown at the bottom of Fig 4 for C18. Since the reflectivity for the C10 sample was only measured for $q \leq 0.65 Å^{-1}$ it was not possible to determine either the parameters appropriate to the SiO_2 layer from this data set or the hydrocarbon electron density, the fit thus being carried out by assuming the SiO_2 layer for this sample was the same as those of all of the other samples studied. The best parameters for both the C10 and C12 fits are listed in Table II and the real-space densities are shown in Fig. 11. Using 96 data points in the range $0.15 Å^{-1} \leq q \leq 0.8 Å^{-1}$, with 6 adjustable parameters, the χ^2 for the C12 fit was 13. The fit for the C10 sample used 62 data points between $0.18 Å^{-1} \leq q \leq 0.65 Å^{-1}$, and with 4 adjustable parameters the χ^2 was 9.4. The confidence limits for the

parameters listed in Table II were set by determining the range of values that increased the χ^2 by 25% over the previously stated minima in the same manner as was previously described in regard to the fits for the C18 sample.

The real-space densities for the $N=3^{(+)}$ models that provide the "best fit" for the C10, C12 and C18 coated wafers are displayed superposed on one another in Fig. 11d. The graphs shown in Fig. 11 suggest that the SiO_2 region for the C10 and C12 samples might be ~1Å shorter than that of the C18 wafer. However, since the data for $q \geq 0.5 Å^{-1}$ is of much lower quality for the C10 and C12 than for the C18 sample, we do not, however, believe this difference is necessarily significant. The graphical determinations of the thicknesses of the alkane region for the C10 and C12 samples are listed in Table II. From these, we obtain a length per carbon atom of 1.38±0.2Å,1.23±0.04Å and 1.18±0.02Å for the C10, C12 and C18 monolayer respectively that can be compared with the accepted value for the 1.265Å for the maximum extension of a fully extended aliphatic chain in the all trans configuration.[41] Although the C18 value is slightly shorter, the three results are identical within the quoted errors. This length for the C18 indicates that there could be either a small degree of gauche isomerization or a tilt in the mean axis of the chains with respect to the surface normal. The result allows the layer thickness to be reduced by no more than 10% from the expected length of an all-trans chain oriented normal to the surface. The data are not sufficient to support or deny a model in which either the gauche isomerization, or the tilt of the chain axis, was larger for the C18 than for the shorter chains.

As a measure of the packing of the monolayers, it is interesting to calculate the area per alkylsiloxane molecule. Given a length per CH_2

group of 1.20±0.05Å for the C12 and C18 monolayers, a silicon electron density of 7.04×10^{23} electrons/cm^3, a hydrocarbon electron density of 0.42±0.02 of that of silicon and that there are 8 electrons per CH_2 group, one obtains an area/alkylsiloxane molecule of 22.5±2.5Å^2. This area should be compared to an area of 20.5Å^2 for long chain paraffins in bulk[44] and between 20.5 to 22.5Å^2 for Langmuir-Blodgett monolayers of long chain alcohols.[45]

Fig. 12 shows the reflectivity from an incomplete C18 alkylsiloxane film, formed by allowing the sample to sit in the solution for a time shorter than that needed to form a full layer of alkylsiloxane. The position of the minima at $q \approx 0.2$Å^{-1}, in comparison with 0.13Å^{-1} for the fully formed C18 film clearly indicates that this alkylsiloxane film is considerably shorter (i.e. 16.2Å) than the fully formed layer (23.5Å). The sample reflectivity also falls off much faster than either that of the fully formed C12 layer with comparable thickness to this partially formed sample, or to the thicker fully formed C18, suggesting that the alkane/air interface is considerably more diffuse for the partially formed layer than for either of the two potentially similar systems. Detailed analysis of the results using the N=3$^{(+)}$ model (using the silicon oxide layer parameters from previous fits to obtain a fit with a χ^2 of 32 for points above 0.15Å^{-1}) indicate the alkane/air interface is characterized by $\sigma_{34} \approx 5.0$Å rather than 2.0-4.0Å for fully formed alkylsiloxane samples. Note that since the data are sensitive to the square of σ_{34}, this difference is well outside of the uncertainties associated with the different models. Since the hydrocarbon/air interface is wider than the silicon oxide/hydrocarbon interface, the graphically measured length of 17.2Å is larger than measured directly from the first minimum position. In this case the graphical method may not accurately determine the mean

hydrocarbon thickness. The parameters for this fit are listed in Table II and the fit is illustrated by the solid line in Fig. 12.

That the electron density of the partially formed layer is comparable to the density obtained for the fully formed layer suggests that the alkane chains either tilt, or otherwise bend, to fill space in order to maintain a density close to the fully formed hydrocarbon density of approximately 0.85 gm/cm^3. If the partial monolayer was comprised of close packed, uniformly tilted, straight C18 chains the mean tilt would be about 45° if one uses the lengths obtained from the dip position or 36° using the graphically determined length. These results are not consistent with one previously suggested model of partially formed films as islands of close packed, straight, fully extended molecules that are oriented normal to the surface.[46,47] The average electron density for this model would consist of a layer of the same length but a lower electron density. Variations of this model, in which the molecules at the boundary of the islands were partially disoriented, would increase the apparent interfacial width σ_{34}, but would not change the thickness.

Fig. 13 shows the comparison of the alkylsiloxane lengths as measured by ellipsometry and from $2\pi/q_{min}$, where q_{min} is the position of the first minimum in the x-ray reflectivity. The ellipsometric measurements will be described in more detail in a separate publication.[34] The x-ray measurements were made using both the rotating anode and synchrotron sources. Assuming a constant offset, the average difference between the ellipsometrically determined length and $2\pi/q_{min}$ corresponds to 1.8±1.0Å with the ellipsometric value being larger. Since the graphically determined value for the x-ray determined thickness is of the order of 1.5±0.6Å shorter than $2\pi/q_{min}$, the ellipsometric values are of the order of 3.0Å larger than the graphically determined values. This difference is slightly outside of the quoted errors of approximately ±0.5Å in the x-ray and ±2Å for the ellipsometrically measured lengths and may be systematic, having an origin in factors such as the effects of the interface on either technique, size related corrections to the index of refraction for the ellipsometric technique, etc.

Table II: Parameters for the N=3(+) models that obtain the best representations of the reflectivity for samples as discussed in the text.

		C10	C12	C18P	C17(=)	C17(Br)•	CF
Layer thickness L_j(Å)							
SiO_2	L_1	16.0±1.5	16.6±0.8	17.0*	12.7±2.5	12.7*	16*
Interface	L_2	1.3±1.5	0.6±0.6	$0.4^{+3.0}_{-0.4}$	6.1±1.5	6.1*	2.0
-(CH_2)-	L_3	13.0±0.3	15.6±0.2	16.5±1.0	20.1±1.5	23.7±0.2	0.1
-(CF_2)-	L_4	----------	----------	----------	----------	----------	12.0
-(CH_2)- gr.	L_3	13.8±2.0	14.8±0.5	17.2±0.4	19.9±0.4	----------	18±2§
ρ_j/ρ_o							
SiO_2	ρ_1	0.97*	0.97±0.01	0.98±.01	0.98±0.01	0.98*	0.98*
Interface	ρ_2	$0.30^{+15}_{-0.08}$	$0.18^{+10}_{-0.15}$	$1.13^{+5.0}_{-0.15}$	0.78±0.15	0.78*	0.43*
-(CH_2)-	ρ_3	$0.41^{*+0.2}_{-0.04}$	$0.41^{+0.04}_{-0.02}$	0.40±0.08	0.41±0.02	0.41*	0.77
-(CF_2)-	ρ_4	----------	----------	----------	----------	----------	0.80
$\sigma_{i,j}$ (Å)							
Si/SiO_2	σ_{01}	1*	1*	1*	1*	1*	1*
SiO_2/Inter	σ_{12}	$4.2^{+1.0}_{-0.2}$	3.3±0.5	1*	2.2±1.2	2.2*	4.2
Int/(CH_2)	σ_{23}	1*	1*	3.4±1.5	3.4±1.2	3.4*	2.8
(CH_2)/Air†	σ_{34}	3.8±0.3	2.9±0.3	3.9±0.9	3.0±0.2	2.1±0.5	1*
(CF_2)/Air	σ_{45}	----------	----------	----------	----------	----------	2.9

*Parameters kept fixed during fitting

•L_{Br}= -4.8±0.6Å, σ_{Br}=2.4± 0.4Å, n_{Br}= 1.40±0.15(Åρ/ρ_o)

§Combined length of the fluorocarbon and hydrocarbon chains.

†For the fluorocarbon sample CF this is the (CH_2)/(CF_2) interface

Other Samples

Bromination of Alkene Terminated Sample

This sample was prepared initially as a π-bond terminated siloxane sample with 18 carbon atoms (i.e. Si-$(CH_2)_{15}$-CH=CH_2). The data, in the form of $R(q)/R_F(q)$, and the calculated results for the $N=3^{(+)}$ model are shown in Fig. 14a (with a χ^2 of 33 for the points above 0.1Å^{-1}). The parameters for the fit are displayed in Table II in the column $C17^{(=)}$ and the real-space electron density is illustrated by the broken line in Fig 15. The reflectivity data are substantially the same as for the simple alkane samples with a somewhat more diffuse hydrocarbon/air interface (3.1Å versus approximately 2.5Å for the simple C18 molecule of similar length) but aside from this difference, there are no systematic differences between the real-space electron densities extracted from this data set and the one for the C18 sample.

After the initial x-ray measurement, the same sample was brominated and measured again (Fig 14b). Bromination results, to a first approximation, in breaking the terminal π-bond and attaching two bromine atoms to the two terminal carbon atoms to give the structure -Si-$(CH_2)_{15}$-CHBr-CH_2Br. Relative to the data in Fig. 14a the overall reflectivity has increased suggesting the presence of additional electron density at the surface, and the position of the first minimum has shifted to a lower angle as would occur if the distance between surfaces were increased.

More detailed fitting was carried out by considering the addition of a single Gaussian to the real-space electron density profile, to account for the bromine electron density, to the $N=3^{(+)}$ model that described the $C17^{(=)}$ data. The three new adjustable parameters in fitting the $C17^{(=)}$ data were the

position:

$$D_{Br} \equiv \sum_{i=1}^{3} L_i + L_{Br},$$

the width σ_{Br} and the area n_{Br} of the Gaussian. The fit was carried out by holding fixed all of the other parameters at the values in column $C17^{(=)}$ of Table II and allowing L_3, L_{Br}, σ_{34}, σ_{Br}, and n_{Br} to vary. The values for the parameters that gave the best fit are listed in column $C17^{(Br)}$ of Table II and in the notes below the Table (χ^2 for the fit of 60 using the points above $0.1 Å^{-1}$). The solid line in Fig 15 displays the real-space electron density for the $C17^{(Br)}$ sample that gave rise to the model reflectivity illustrated by the solid line in Fig. 14b. From Fig. 15 it appears that the additional electrons associated with the bromine atoms reside close to the end of the hydrocarbon chain, their presence extending the overall thickness of the monolayer.

If A_o is the average cross sectional area per alkylsiloxane group, ρ_o is the electron density of crystalline silicon and N is the additional area under the electron density profile associated with adding the bromine group, the product $N\rho_o A_o$ is equal to the number of extra electrons per surface alkylsiloxane group. From the parameters of Table II which indicate an additional $(0.41 \times 3.6 + 1.4)Å/\rho_o$ and using $\rho_o = 7.04 \times 10^{23}$ electrons/cm^3 and the previously obtained area/alkylsiloxane molecule of $22.5 \pm 2.5 Å^2$ one calculates the addition of 45±10 electrons per alkylsiloxane group. Assuming that bromination takes place as described above, the fully brominated layer would have 66 effective electrons per alkylsiloxane (the two 1s electrons per bromine atom are too tightly bound to contribute to the measured electron density). This measurement thus implies that only 45/66, or 68% of the molecules were brominated.

XPS analysis carried out some weeks later than the x-ray measurement showed that on sections of the sample which were not in the beam 90% of the molecules were brominated but on radiated sections this figure was only about 30%. It is clear that the radiation had initiated some chemical change to the monolayer surface. Damage occurred during the x-ray exposure both before and after bromination. This damage is probably visible in the reflectivity scans shown in Fig. 14 as a pairing of points at large scattering vectors that were taken about 30 minutes apart, the later points being shown solid. It is, however, also possible that the observed changes in the x-ray reflectivity have a different origin. While this implication of x-ray damage adds some uncertainty to the significance of the x-ray determined of the electron densities in this sample, it does not alter the basic objective of demonstrating that specular reflection can be used for quantitative determination of chemical modifications of the alkane surface.

Fluorocarbon Coated Sample.

In order to demonstrate the applicability of the technique to samples with a radically different layer density from the hydrocarbon, a wafer was coated with a monolayer of $-Si-(CH_2)_2-(CF_2)_7-CF_3$. The reflectivity data for this sample, in the form of $R(q)/R_F(q)$ and the calculated results for a N=4 model are shown in Fig.16a. Since the difference in electron density between the silicon-oxide and the fluorocarbon layers is much less than that between the silicon-oxide and the alkane layer in the previous samples, the amplitude of the x-ray reflected from the fluorocarbon/air interface is correspondingly stronger than the net amplitude reflected from the composite interface between the fluorocarbon/silicon-oxide interface. As a consequence the depth of the first interference minima at $q \approx 0.2 Å^{-1}$ is much

shallower in this sample than the corresponding minima for the alkane coated samples. On the other hand, since the amplitude of the signal reflected from the fluorocarbon-air interface is greater than amplitude of the signal from the composite interface, and since that is yet larger than the amplitude reflected from the Si/SiO_2 interface, the interference pattern is dominated by the two signals from the first two interfaces. As a result, the two minima at $q=0.18Å^{-1}$ and $0.55Å^{-1}$ in Fig. 16a correspond to roughly $qL = \pi$ and 3π with $L\approx17.8Å$. We suggest that this is the distance between the silicon-oxide/$(CH_2)_2$ and the fluorocarbon/air interface. This should be compared to a length of 18.1Å obtained from the graphical analysis of the four layer fit.

The one unfortunate consequence to follow from the fluorocarbon electron density is that the reflectivity is less sensitive to the SiO_2 layer and its two interfaces. The solid line in Fig16a is calculated from a model in which N=4, but using values for the parameters describing the SiO_2 layer, its interfaces and other parameters for the hydrocarbon portion of the molecule as determined from the other samples. In addition, since the data was only taken for $q\leq0.7Å^{-1}$, and since the points near $q\approx0.7Å^{-1}$ themselves have large error bars, the confidence limits on the fit parameters are larger than those for the other fits. In any event, the parameters that obtained the best fit and are physically realistic are displayed in Table II. The real-space electron density is shown in Fig. 16b. The solid line indicates the 17.8Å that is the origin of the principle interference minima in Fig. 16a.

DISCUSSION.

The very deep nature of the first interference minima for the hydrocarbon samples with well formed films is a direct demonstration that organic monolayers synthesized by the self-assembly process are capable of providing microscopically and macroscopically uniform films. In particular, the first sharp minima in the reflectivity allows an immediate determination of the thickness of the adsorbed film that is in reasonable agreement with the thicknesses predicted by assuming maximally extended aliphatic chains normal to the surface, when the size of the silicon head group is assumed to be included in the length measured. Comparisons between x-ray reflectivities calculated from several detailed models of the film, including modeling of the head region, allowed an estimate of the length of the hydrocarbon thickness. This thickness suggests that the molecules are close to being maximally extended. The principle residual uncertainty of the hydrocarbon thickness is due to the width of the interfacial region between the SiO_2 layer and the hydrocarbon layer. We suspect that the major contribution to this is the roughness of the bare SiO_2 substrate and that a significant improvement could be obtained by preselection of flatter substrates.

The highly sensitive dependence of the reflectivity on details of the monolayer is indicated by the much improved fits of the N=3 model as compared to the N=2 model, the differences being only small changes in the electron density profile at the silicon oxide/alkylsiloxane interface. The reflectivity is particularly sensitive to the interface width, which must be considered separately for each of the interfaces if a good fit to the data is to be obtained. This sensitivity to interfacial structure has been neglected in most other x-ray studies of similar systems.

In spite of some problems with contamination from airborne hydrocarbons, a reasonable characterization of the bare SiO_2/air interface prior to the self-assembling process yields a root mean square Gaussian width of the order of 2.8Å. This is slightly smaller than the width of the hydrocarbon/air interface for the C18 sample; however, for some other samples the width of this interface is slightly larger. Inspection of the various models for the C18 real-space electron density (i.e. Fig. 6) suggest the hypothesis that the real-space density might be the result of coating the SiO_2 surface, which has some roughness, with a fixed thickness of alkane. The variations in the model parameters for the width of the SiO_2/alkane and alkane/air interfaces leads to some uncertainty in the thickness to the alkane layer. However, from the graphical inspection of the various models described earlier, we believe this is no more than on the order of ±0.5Å (1.0Å for the C10 alkylsiloxane). Using the thickness of the hydrocarbon part of the C18 molecule only, the measured tilt angle is about $\cos^{-1}(21.4/(1.265 \times 18)) = 20°$. Uncertainty in the hydrocarbon thickness places an uncertainty of about ±4° on this result.

In summary, the x-ray data is consistent with uniform monolayers whose thicknesses are of the order of 95% of the expected values for maximally extended alkane chains normal to the surface. The layer thicknesses determined directly from the dip minimum in the x-ray specular reflectivity also agree within 2Å with those determined by ellipsometric measurements. Since the width of the head group affects the position of the minimum, we believe, however, that the thickness of the alkane region alone may be as much as 4Å thinner than the ellipsometrically quoted values.

The structure near the silicon oxide/hydrocarbon interface is almost certainly due to the silicon-oxygen network formed by the siloxane head groups to neighboring atoms and to the silicon oxide surface. Since the available data are restricted to a region of $q \leq 0.8 Å^{-1}$ we did not have sufficient resolution to distinguish between a well-formed head group layer, at a fixed distance from the SiO_2 substrate, or one that is more distorted. From the absence of any chlorine signal in the XPS spectra we can, however, be confident that the interface structure is not due to chlorine atoms remaining from the preparation.[40]

The electron density of the fully formed alkylsiloxane layers was essentially independent of the sample, having values between 0.41 and 0.43 of the silicon electron density. This value is equivalent to a mass density of between $0.83 g/cm^3$ and $0.87 g/cm^3$ (silicon has a mass density of $2.33 g/cm^3$). This is somewhat larger than densities of liquid phases of alkanes containing 12 to 18 carbon atoms ($0.75 g/cm^3$ and $0.78 g/cm^3$), but it is less than the densities found for crystalline phases of the same materials ($0.93 g/cm^3$).[44] This is essentially a restatement of the previous calculation in which the area per hydrocarbon chain was found to be approximately 10% larger than that of crystalline alkanes. It appears that the self assembling process at the Si/SiO_2 surface forces a packing of the alkane chains that is denser than liquid alkane phases but less dense than the crystalline alkane.

The width of the hydrocarbon/air interface does vary considerably between the long and short hydrocarbon chains, with values of 3.8, 2.9 and 2.4Å for the C10, C12 and C18 alkylsiloxanes respectively (see Fig. 11). This may be due to the increased flexibility of the longer chains which are able to

deform more easily and thereby quench some of the non-uniformity introduced at the silicon oxide/hydrocarbon interface.

The most striking feature of the partially formed C18 alkylsiloxane reflectivity data when compared to the fully formed layer is the change in the position of the first minimum, unambiguously indicating a reduced thickness of the incomplete monolayer. Since the average electron density in the alkane layer is essentially the same as that for all of the fully formed layers, this result absolutely rules out the previously suggested model of islands of fully extended molecules.[32] For films thinner than approximately 100Å ellipsometry is only sensitive to the mean optical thickness, ruling out the possibility of distinguishing between the island hypothesis and the uniform layer. The reduced thickness of the partially formed layer could be explained in terms of an homogeneous coating in which the mean molecular tilt was about 45°. However since the alkane/air interface for the incompletely formed monolayer was also found to be rougher than the same interface for all of the fully formed film monolayers the correct description of the partially formed monolayer must involve some degree of non-uniformity in the coating.

The present set of measurements cannot distinguish between a uniform-diffuse interface and one that was microscopically sharp, but rough. In principle, this distinction could be made by a more systematic study of the line shape as ϕ is tuned off of the specular condition, like those shown in Fig. 3, but using a much finer resolution such as can be obtained using a crystal analyzer.[14] Nevertheless, one very important result of these series of measurements is the observation that the data will not support a value for the parameter σ_{01} that describes the Si/SiO_2 interface that is greater than 2Å. The fitting algorithm always drives it to zero.

A variation of the technique described here is to study the way the intensity falls off as the spectrometer is tuned away from the condition for Bragg reflection, rather than away from the condition for specular reflection. The intensity along the "truncation rods"[48,49] can be interpreted in terms of the width of the termination of the crystal lattice, rather than as we have done in terms of the the density profile at the interface between two regions of differing average electron density. The data for the surface of crystalline silicon indicates that the silicon lattice termination occurs in a single step, giving an atomically flat silicon/silicon oxide interface.[48,49] Another study using transmission electron diffraction on specially prepared silicon wafers also found prefect termination of the silicon crystal lattice.[50] A 5Å layer of ordered silicon oxide crystal was found at the crystalline silicon/amorphous silicon-oxide interface. Our measurements are consistent with these results indicating a very narrow silicon/silicon oxide interface, although more detailed investigation of a different system will be needed to provide more information about this interface given the short length scales involved. This interface, and in particular its width, is of exceptional importance to the silicon- based electronics industry.[42,51]

Using other, more intense synchrotron beam lines, it should be straightforward to extend x-ray reflectivity measurements to values of q at least two or three times larger than the maximum of $0.9Å^{-1}$ in the present measurements. Provided neither radiation damage nor diffuse background radiation are the limiting features, this would allow characterization of the structure of the various interfaces to a spatial resolution that could be three times finer than achieved in the present measurement. Furthermore, if the Si/SiO_2 sample was protected from airborne contaminants, specular reflectivity measurement of the bare

Si/SiO_2 substrate is the only method of which we are aware that has the potential for fully characterizing the transition from the crystalline silicon region, through the strained crystalline Si/SiO_2 region, into the region of amorphous SiO_2.

In some respects the use of the Si/SiO_2 substrate, with its native oxide layer, complicated the analysis and made it more difficult to characterize the alkane surfaces. On the other hand, the Si/SiO_2 substrates have the decided advantages of having a much sharper interface with air than any other solid surface of comparable dimensions that we could obtain. In addition, since the observed diffuse scattering from the Si/SiO_2 samples, at all angles of incidence, is significantly lower than that observed from highly polished amorphous materials (such as polished or float glass), we believe that the microscopic surface width of the Si/SiO_2 surface is also significantly less than for other possible substrates.

The data on the olefin-terminated C18 sample, together with the study on the effect of bromination, illustrate a powerful tool for study of certain types of surface chemistry. In this particular example Br_2 molecules added to the reactive olefin groups attached to the end of the alkyl chains. From the x-ray reflectivity, it was possible to observe the position of the Br atoms and the consequent distribution of the electron density. Although there were some effects of radiation damage that were discovered after the x-ray measurements were completed, the example suggests that this type of measurement could be carried out using a much larger variety of reactive species. In particular, if the moiety to be attached to the end of the alkane group has some extended structure, this technique would allow for a relatively detailed mapping of its electron density. Since the specular reflection from the substrate provides a reference field this technique has a

built in solution to the phase problem that plagues most other x-ray techniques for structural determination.

The most serious limitation on the potential applicability of specular reflection for the study of organic monolayers is the problem of radiation damage. In the present work most of the samples with well formed alkanes had a contact angles with water of approximately 110° before synchrotron reflectivity measurement and from 80° to 95° afterwards depending on the amount of exposure. XPS studies of the irradiated region suggested between 5-20% of the alkyl chains had been oxidized forming either C-OH or C=O groups, while sections of the sample that were not irradiated did not show the presence of any C-O bonds.[34] This damage was not observed on samples measured during experiments using the rotating anode with filtered radiation (where x-ray exposure was roughly 1% of the synchrotron exposure), but was reproduced when a sample was exposed to the polychromatic beam for 24 hours. In a few cases there was some evidence that for $q \geq 0.7 Å^{-1}$ radiation damage may have been observed as changes in the reflectivity of the order of 30%, however no changes were detected for $q \leq 0.5 Å^{-1}$.

Since only about 0.1 photons per alkyl group fell on the sample during the course of a typical series of scans, with most being transmitted into the silicon bulk, and given that the number of damaged molecules exceeds this number, the damage cannot be associated with the photoelectric effect acting directly on the alkylsiloxane molecules. One possibility is that the damage is induced by photoelectrons generated by x-rays in the silicon substrate. These KeV energy electrons interact strongly with other electrons spawning many more secondary electrons which could ionize the carbon atoms in the alkylsiloxane chain. The final damage would then

result when highly reactive radicals thus formed combine with oxygen in the surrounding air. Alternatively, x-ray induced ozone in the atmosphere might be the source of the damage, or there might be free-radical chain reactions mediated by oxygen in the organic monolayers.

There are a number of ways that this damage might be reduced. Firstly, and most obvious would be to place the sample in an atmosphere free of O_2. Secondly, the measurements can be managed with significantly less exposure to radiation than was the case in these studies. For example, measurements of background scattering do not necessarily have to be taken with the same statistics as for the main data. In any event the background scans can be taken after the reflectivity data has been completed. Since the background is mainly due to air and bulk scattering, it will be little affected by surface damage. The exposure can also be reduced by optimizing the number of data points to eliminate much of the redundancy evident in the data in Fig. 1 at low angles. In addition, since the samples have proven to be highly uniform, and very reproducible, data points can be taken on the different regions of the wafer.

Finally, changes in the reflectivity with time that were measured on the uncoated silicon sample are probably due to the build up of contamination on the surface. As discussed above, accumulation of contamination is evident in Fig. 1a as the pairing of points at large angles and the movement (not shown) of the dip at $q \approx 0.6 Å^{-1}$ to lower angles at later times. The dip and its time development suggest the build up of a contamination layer on the surface with a density lower than silicon. The build up of this layer is due to the high energy of the Si/SiO_2 surface (several hundred erg/cm^2 compared to about 20 erg/cm for the coated surfaces).[33] The strong signal from this layer makes it difficult to characterize the SiO_2

layer from the data in Fig. 1a. Future measurements of the uncoated Si/SiO_2 surface must be done under more rigorously atmospherically controlled conditions that were available for this study.

ACKNOWLEDGEMENTS

The authors express their thanks to D. Osterman for help during the work at NSLS. This work was supported by the National Science Foundation through grants to the Harvard Materials Research Laboratory, NSF-DMR-85-13523 and -86-14003, from the Joint Services Electronics Program of the Department of Defense though grant N0014-84-K-0465 and from ONR/DARPA grants N00014-83-K-0142 and -85-K-0898. Research carried out at the NSLS, Brookhaven National Laboratory, is supported by the Department of Energy, Material Sciences and Division of Chemical Sciences under contract DE-AC02-76CH00016. One of us (I.M.T.) would like to acknowledge support from a NATO studentship.

References.

[1]A. H. Compton, Bull. Nat. Res. Coun. (US) **20**, 48 (1922).

[2]L. G. Parratt, Phys. Rev. **95**, 359 (1954).

[3]B.C. Lu and S. A. Rice, J. Chem Phys. **68**, 5558 (1978).

[4]D. Sluis and S. A. Rice, J. Chem. Phys. **79**, 5658 (1983).

[5]L. Bosio and M. Oumezine, J. Chem Phys. **80**, 959 (1984).

[6]L. Bosio, R. Cortes, A. Defrain, and M. Oumezine, J. Non-Cryst. Solids **61&62**, 697 (1094).

[7]R. A. Cowley and T. W. Ryan, J. Phys. D: Appl. Phys. **20**, 61 (1987).

[8]M. Pomerantz , A. Segmuller, L Netzer and J. Sagiv, Thin Solid Films **132**, 153 (1985).

[9]M. Pomerantz and A. Segmuller, Thin Solid Films **68**, 33 (1980).

[10]R. M. Richardson and S. J. Roser, Liquid Crystal **2**, 797 (1987).

[11]J. Als-Nielsen, F. Christensen and P. S. Pershan, Phys. Rev. Lett. **48**, 1107 (1982).

[12]P. S. Pershan and J. Als-Nielsen, Phys. Rev. Lett. **52**, 759 (1984).

[13]B. M. Ocko, A. Braslau, P. S. Pershan, J. Als-Nielsen and M. Deutsch, Phys. Rev. Lett. **57**, 94 (1986).

[14]P. S. Pershan, A. Braslau, A. H. Weiss and J. Als-Nielsen, Phys. Rev. A **35**, 4800 (1987).

[15]P. S. Pershan, Proc. Natl. Acad. Sci. **84**, 4692 (1987).

[16]E. F. Gramsbergen, W. H. de Jeu and J. Als-Nielsen, J. Physique **47**, 711 (1986).

[17]D. K. Schwartz, A. Braslau, B. M. Ocko, P. S. Pershan, Phys. Rev. A *To be published (1988).*

[18]A. Braslau, M. Deutsch, P. S. Pershan, A. H. Weiss, J. Als-Nielsen and J. Bohr, Phys. Rev. Lett. **54**, 114 (1985).

[19]A. B. Braslau, P. S. Pershan, G. Swislow, B. M. Ocko and J. Als-Nielsen, Phys. Rev. A **38**, 2457, (1988).

[20]F. Rieutord, J. J. Benattar and L. Bosio, J. Physique **47**, 1249 (1986).

[21]S. G. Wolf, L. Leiserowitz, M. Lahav, M. Deutsch, K. Kjaer and J. Als-Nielsen, Nature **328**, 63 (1987).

[22]C. A. Helm, H. Möhwald, K. Kjaer and J. Als-Nielsen, Europhys. Lett. **4**, 697 (1987).

[23]B. M. Ocko and S. J. G. Mochrie, Phys. Rev. B *To be Published (1988).*

[24]D. GIbbs, B. M. Ocko, D. M. Zehner and S. J. G. Mochrie, Phys. Rev. Lett. *To be Published (1988).*

[25]K. B. Blodgett and I. Langmuir, Phys. Rev. **51**, 964 (1937).

[26]J. D. Swalen *et al*, Langmuir **3**, 932 (1987).

[27] J. Sagiv, J. Am. Chem. Soc. **102**, 92 (1980).

[28] L. Netzer, R. Iscovici and J. Sagiv, Thin Solid Films **99**, 235 (1983).

[29] L. Netzer, R. Iscovici and J. Sagiv, Thin Solid Films**100**, 67 (1983).

[30]R. Maoz and J. Sagiv, J. Coll. Intf. Sci. **100**, 465 (1984).

[31]E. Sabatani, R. Maoz, J. Sagiv and I. Rubinstein, *To Be Published* (1987).

[32]S. R. Cohen, R. Naaman and J. Sagiv, Phys. Rev. Lett. **58**, 1208 (1987).

[33] Contact Angle: Wettability and Adhesion, Ed. F. M. Fowkes, Advances in Chemistry Series **43**, (1964). Article by W. A. Zisman, page 1, and others.

[34] S. R. Wasserman, G. M. Whitesides, I. M. Tidswell, B. M. Ocko, P. S. Pershan and J. D. Axe, J. Am. Chem. Soc., *submitted (1988).*

[35]D. W. Oxtoby and S. A. Rice, J. Chem. Phys **76**, 5278 (1982).

[36]M. Born and E. Wolf, Principles of Optics 6th edition, (Pergamon Press, New York, 1980).

[37] J. Als-Nielsen, Surf. Sci. **140A**, 376 (1986).

[38] Y.Yoneda, Phys. Rev. **131**, 2010 (1963).

[39]S. K. Sinha, E. B. Sirota, S. Garoff and H. B. Stanley, Phys. Rev. B. **38**, 2297 (1988).

[40]S. R. Wasserman, Y-T. Tao, and G. M. Whitesides, Langmuir, *submitted (1988).*

[41]C. Tanford, "The Hydrophobic Effect:Formation of Micelles and Biological Membranes,"(Wiley, New York, 1973) p 52.

[42]K. Sokrates and T. Pantelides, Ed. *The Physics of SiO_2 and its Interfaces* (Pergamon, New York, 1978).

[43]B. E. Warren, *X-Ray Diffraction* (Addison-Wesley, Reading, Massachusetts, 1969), p. 108.

[44]S. C. Nyburg and H. Lüth, Acta. Cryst., **B28**, 2992 (1972).

[45]G. L. Gaines Jr. *Insoluble Monolayers at Liquid-Gas interfaces Interscience*, (New York, 1966) and references cited therein.

[46]S. R. Cohen, R. Naaman and J. Sagiv, J. Phys. Chem **90**, 3054 (1986).

[47]S. Garoff, R. B. Hall, H. W. Deckman, M. S. Alvarez, Proc. Electro. Chem. Soc. **112**, 85 (1985).

[48] S. R. Andrews and R. A. Cowley, J. Phys. C. **55**, 6427 (1985).

[49] I. K. Robinson, Phys. Rev. B **33**, 3830 (1986).

[50] A. Ourmazd, D. W. Taylor, J. A. Rentschler and J. Bevk, Phys. Rev. Lett **59**, 213 (1987)

[51] A. Ourmazd and J. Bevk, Proc. Electronic Soc, *To be Published,* (1988).

FIG. 1.

Normalized reflectivity data from several samples. Successive data sets are displaced by 100x and error bars omitted for clarity. (-) Theoretical reflectivity from an ideal step interface with bulk silicon density. (o) Uncoated silicon sample in Helium; the "pairing" of points occurs for two scans taken 60 minutes apart and is probably due to the build up of contaminants on the surface. (Δ) 10 carbon chain alkylsiloxane. (∇) 12 carbon chain alkylsiloxane. ($\square$) 18 carbon chain alkylsiloxane. The inset shows a schematic diagram of the scattering vectors for the specular reflectivity condition, where $2(\phi)=2\theta$.

FIG. 2.

a) Schematic of the rotating anode configuration. S_2 was the beam-defining slit; the monochromator was either triple bounce or single bounce germanium. All lengths are in millimeters, with typical slit dimensions given in the text.

b) Schematic of the synchrotron configuration (beamline X-22B at NSLS). S_1 defined the coarse horizontal and vertical beam, fine beam definition being obtained from slit S_2; the monochromator was a single-bounce germanium crystal.

FIG. 3.

Three typical beam profiles obtained by scanning 2θ at fixed ϕ for the spectrometer shown in Fig. 2b. The trapezoidal shape is a function of the resolution of the S_4 slit and the beam profile, the former being much larger to ensure all of the reflected beam enters the detector. The lines give the best fit for the amplitude of a trapezoid whose shape was fixed and determined by the incoming beam dimensions and the detector slit width. For all specular scans the detector was positioned in the center of the trapezoid.

FIG. 4.

Reflectivity and analysis of a an alkylsiloxane monolayer containing an 18-carbon chain using one-, two- and three-layer models. The data are shown after normalization to the silicon Fresnel reflectivity, and hence the y axis represents $|\Phi|^2$. Fig. a shows the one-layer model fit to the data at low q. This model accurately fitting only the first minimum; the two-layer fit (b) is quite accurate out to about 0.45Å^{-1} and qualitatively predicts the peak and dip positions at larger angles. The three-layer model (c) reasonably fits the data over the entire range. The best fit parameters for the different models are given in Table I in the N=1, 2 and $3^{(+)}$ columns.

FIG. 5.

Patterson function calculated from the data in Fig. 4 for the 18-carbon chain alkylsiloxane monolayer. The solid curve was calculated directly from the the Fourier transform of the data; the dashed curve was obtained by multiplying the reflectivity data by a Gaussian of the form $\exp(-q^2/2\sigma_p^2)$, where $\sigma_p=0.3\text{Å}^{-1}$, prior to taking the Fourier transformation. Multiplying the data by a Gaussian is equivalent to convoluting the Patterson function with a Gaussian of the form $\exp[-(z-z')^2\sigma_p^2/2]$. The fact that the peak at about 40Å survives the convolution process indicates that it is a real feature of the data and not an artifact of the data termination.

FIG. 6.

Real-space profiles of the model surface electron density from the parameters used to obtain fits in Fig. 4. Figures a, b, and c shows the model profiles for the N=1 (·····), N=2 (----) and N=3 (——) fits. Figure d shows the three profiles overlapping for comparison. The hydrocarbon/air interface and hydrocarbon density and length are similar in all the fits, the only region with significant variation being the silicon oxide/hydrocarbon region. The constructions shown in the three top figures illustrate a graphical technique, which is discussed in the text, for determining the thickness of the hydrocarbon region from these measured densities. The lengths shown as the solid arrows in a,b and c are given in Table I. The dashed line in d shows the length of 23.6Å measured directly from the position of the first minimum in the data shown in Fig.4.

FIG. 7.

Unconvoluted patterson form of the data for the C18 sample (o) together with the Patterson functions for the N=1(·····), 2(- - -) and $3^{(+)}$(——) fits shown in Fig. 4. The two-layer fit includes the peak at 40Å. The round shape of the peak between 20Å and 30Å does not account for the measured reflectivities between $0.4\text{Å}^{-1}\leq q\leq 0.8\text{Å}^{-1}$. Discrepancies between the $N=3^{(+)}$ fit and the data at low s are due to effects of the data termination at $q\approx 0.8\text{Å}^{-1}$.

FIG. 8.

Comparisons of different fits for the C18 sample whose parameters are shown in Table I. a) corresponds to column $3^{(+)}$, b) column $3^{(-)}$, c) column $3^{(+1)}$, and d) column $3^{(+2)}$. The parameters are shown in Table I.

FIG. 9.

Real-space densities corresponding to the fits of the reflectivity scans shown in Fig. 8a-d. Fig. 9a-d show the densities with sharp interfaces. Figs. 9e-f are the corresponding real-space profiles including the widths of the different interfaces. The sharp feature in Fig. 9g is well beyond the resolution limit and a fit that is almost as good would have a profile more similar to Fig. 9e and f. Fig. 9i shows a comparison of the $3^{(+)}$ and $3^{(-)}$ density profiles on the same axes.

FIG. 10A.

Three layer fit and Fresnel normalized reflectivity for a 10 carbon chain alkylsiloxane monolayer. The fit parameters are given in Table II.

FIG. 10B.

Three layer fit and Fresnel normalized reflectivity for a 12 carbon chain alkylsiloxane monolayer. The fit parameters are given in Table II.

FIG. 11.

Real-space profiles for the (a)C10(·····), (b)C12(----), and (c) C18(——) samples obtained from the reflectivity fits. Figure d shows the same profiles overlapping for comparison. Note that although the length of the hydrocarbon layer varies significantly, the silicon oxide layer and layer density are similar for all three samples. The dashed arrows show the length as determined directly from the position of the first minimum. The solid arrows show the construction described in the text used to obtain the revised estimate of the hydrocarbon thickness.

FIG. 12.

Three layer fit and Fresnel normalized reflectivity for a partially formed C18 alkylsiloxane monolayer. The fit parameters are given in Table II.

FIG. 13.

Comparison of the alkylsiloxane length as determined by x-ray reflectivity and by ellipsometry. (o) are fully formed monolayers, (∇) are incompletely formed layers. The solid line corresponds to the expected curve if both techniques gave the same

result. The dashed curve is a fit to the fully formed layer results and has the form $L^{ellip} = 1.02(\pm 0.06) \times L^{x\text{-}ray} + 1.8(\pm 1.1)$Å. The two techniques appear to predict the same length per CH_2 group, but have different sensitivities to the silicon oxide/hydrocarbon interface.

FIG. 14.

Fresnel normalized reflectivity from the olefin terminated sample (a) together with the reflectivity from the same sample after bromination (b). The technique used to fit the data is described in the text, with the parameters for the fits are given in Table II. The filled points at large q indicate the data taken on a second measurement. The small systematic differences may be indicative of the radiation damage observed by the contact angle and XPS measurements.

FIG. 15.

Real-space electron density profile of the the surface obtained from the parameters of the fits in Fig. 14 fcr the alkene sample and the same sample after bromination. Note that the fit to the brominated sample was done by using the parameters of the unbrominated sample (dashed line) for all except the hydrocarbon/air interface. The addition of the peak is due to the addition of the two bromine atoms to the head of each molecule.

FIG. 16.

(a) Normalized Reflectivity and three-layer fit for a fluorocarbon sample. The parameters are shown in Table II. Because of the limited range of data and the complicated nature of the interface it was impossible to obtain accurate values for the parameters, the fit being only a physically reasonable one.

(b) Real-space electron density profile of the surface of the sample obtained from the parameters of Fig. 16a. Note that the fluorocarbon chain has a much higher density than the hydrocarbon chain resulting in the less pronounced first minimum. The dip in the real-space profile corresponds to the location of the two methylene (CH_2) groups in the molecule.

Fig. 1
Tidswell et al.

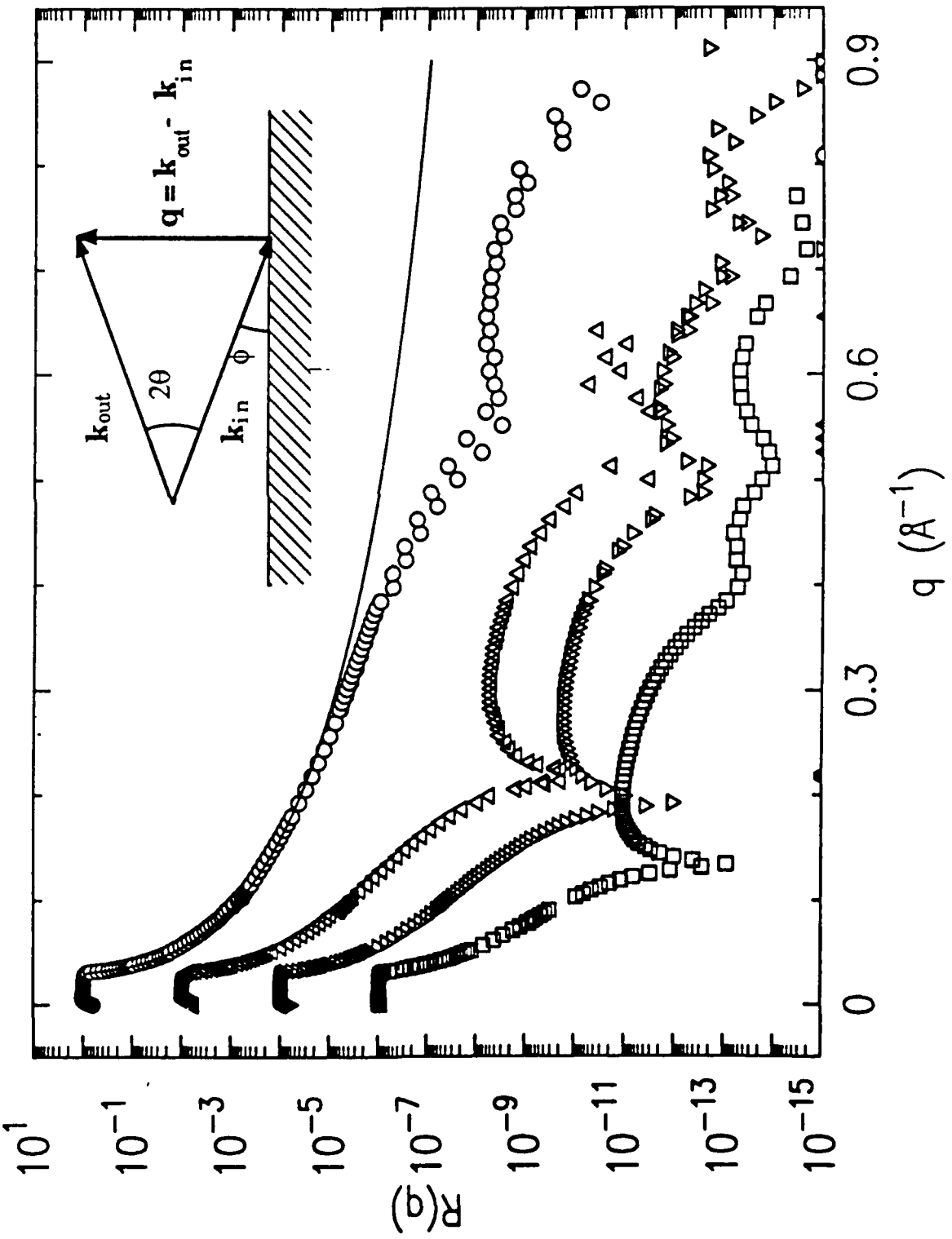

Fig. 2
Tidswell et al.

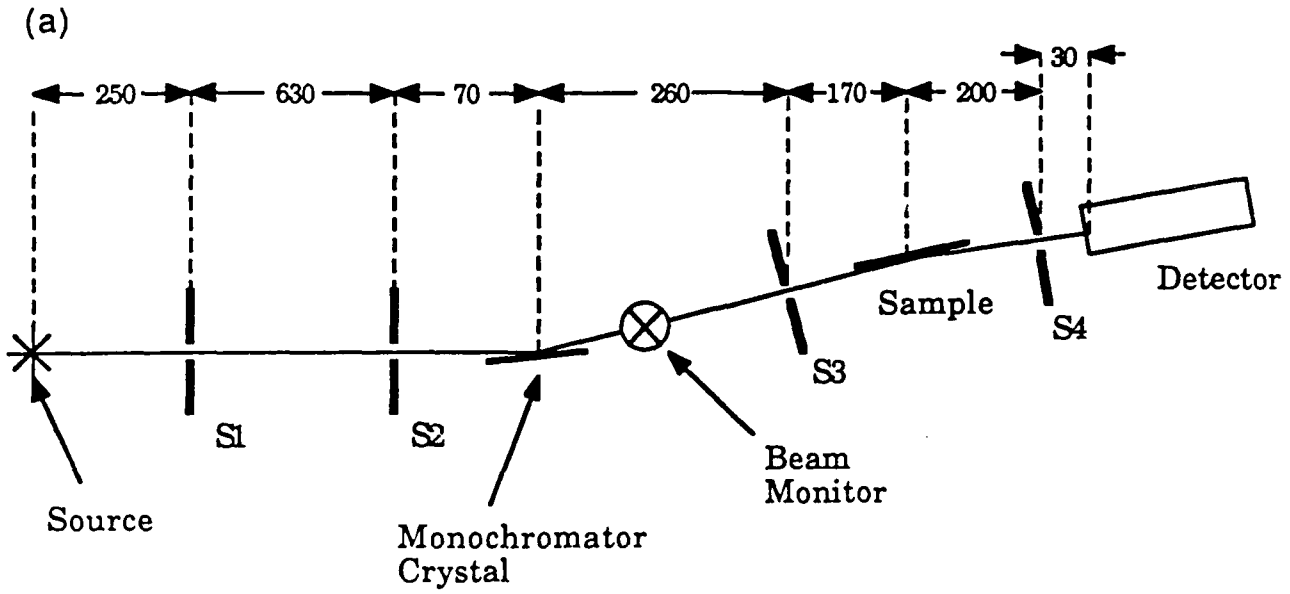

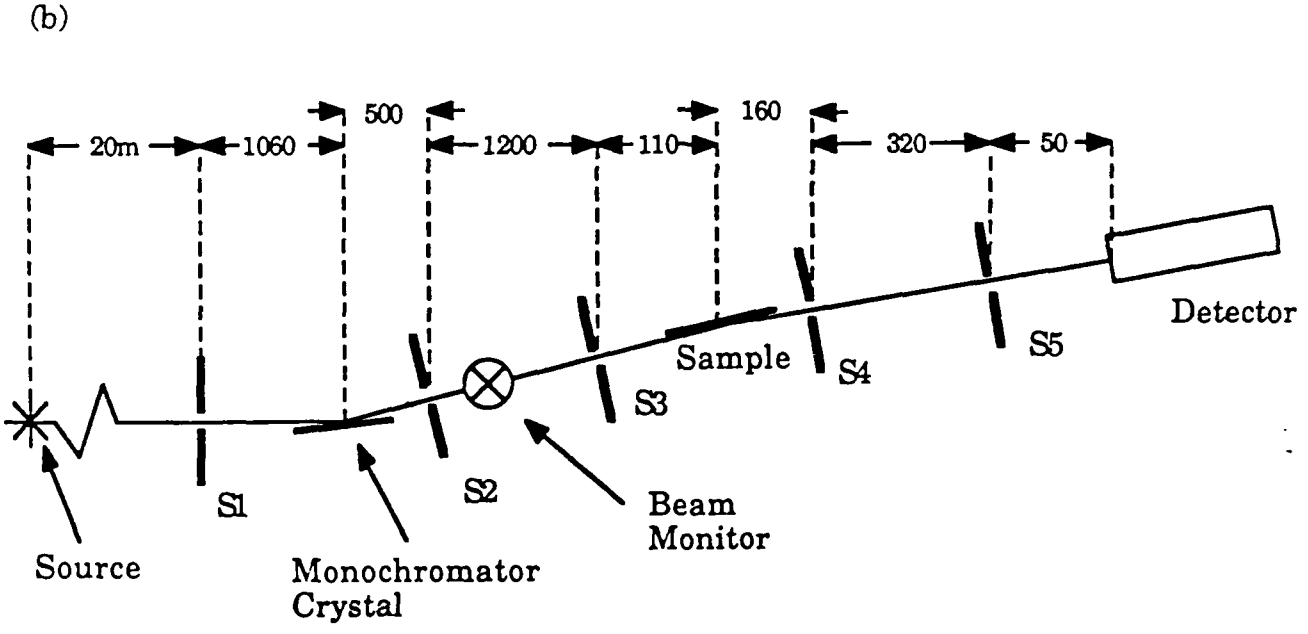

Fig. 3
Tidswell et

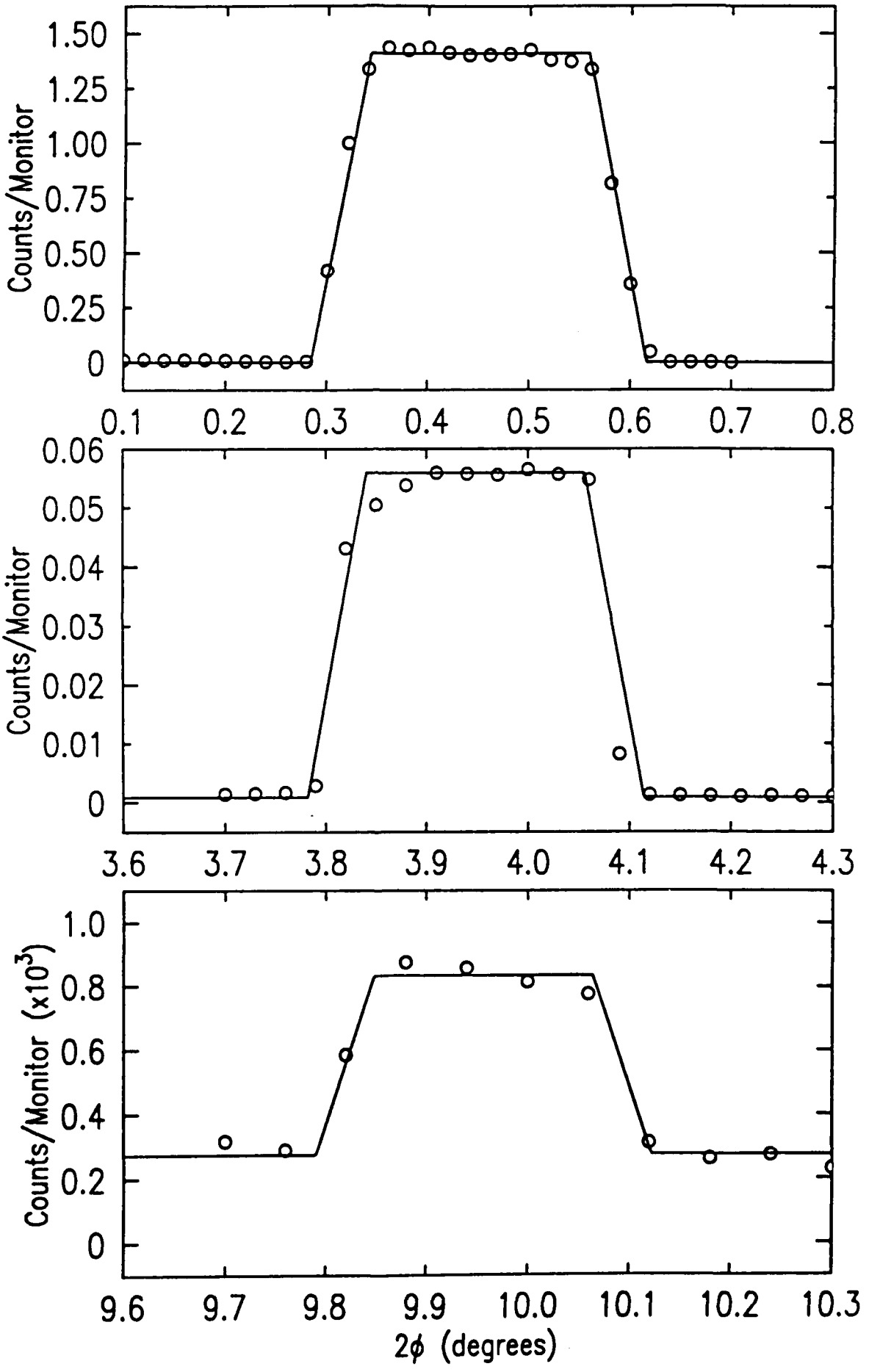

Fig. 4
Tidswell et c

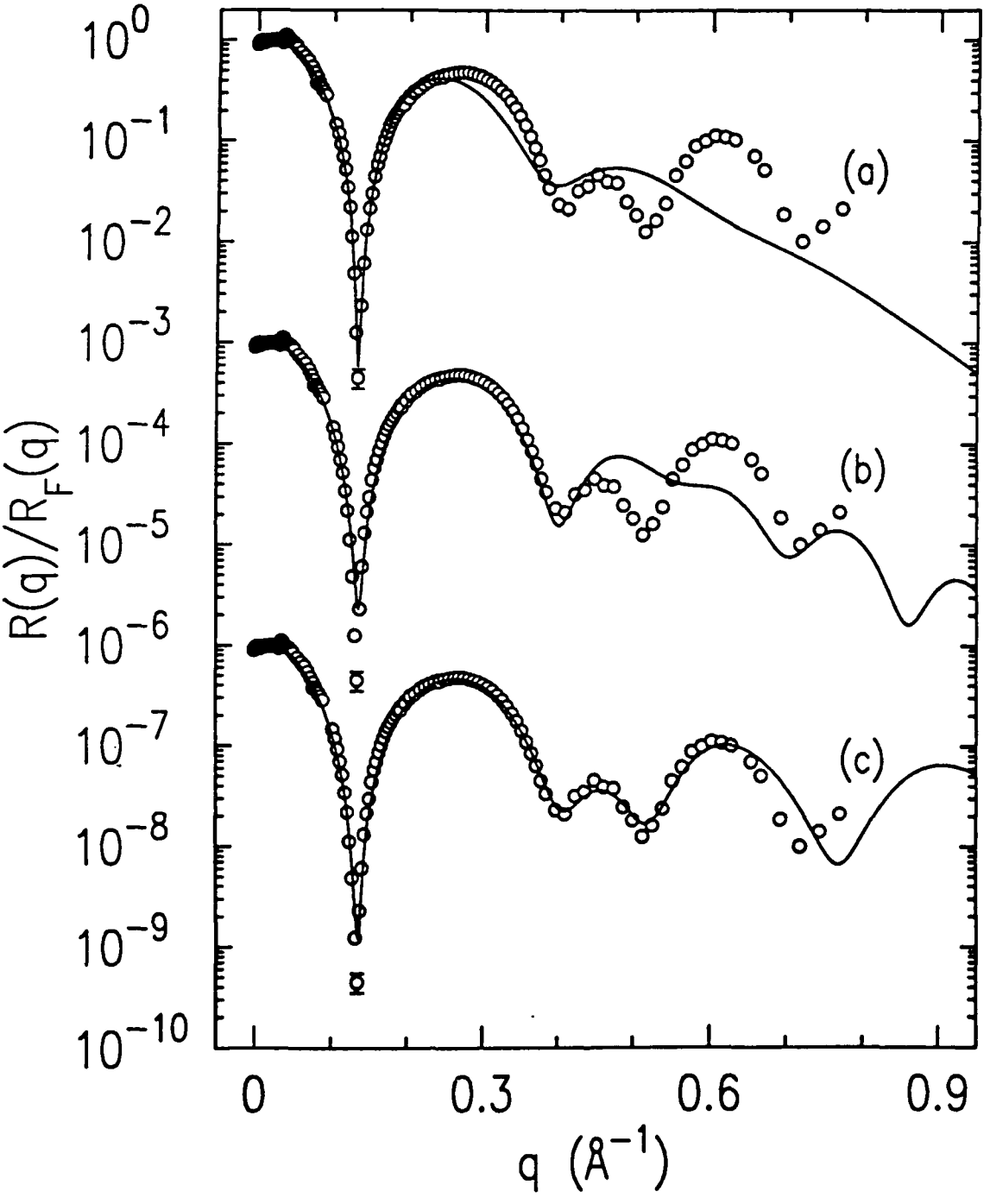

Fig. 5
Tidswell et al

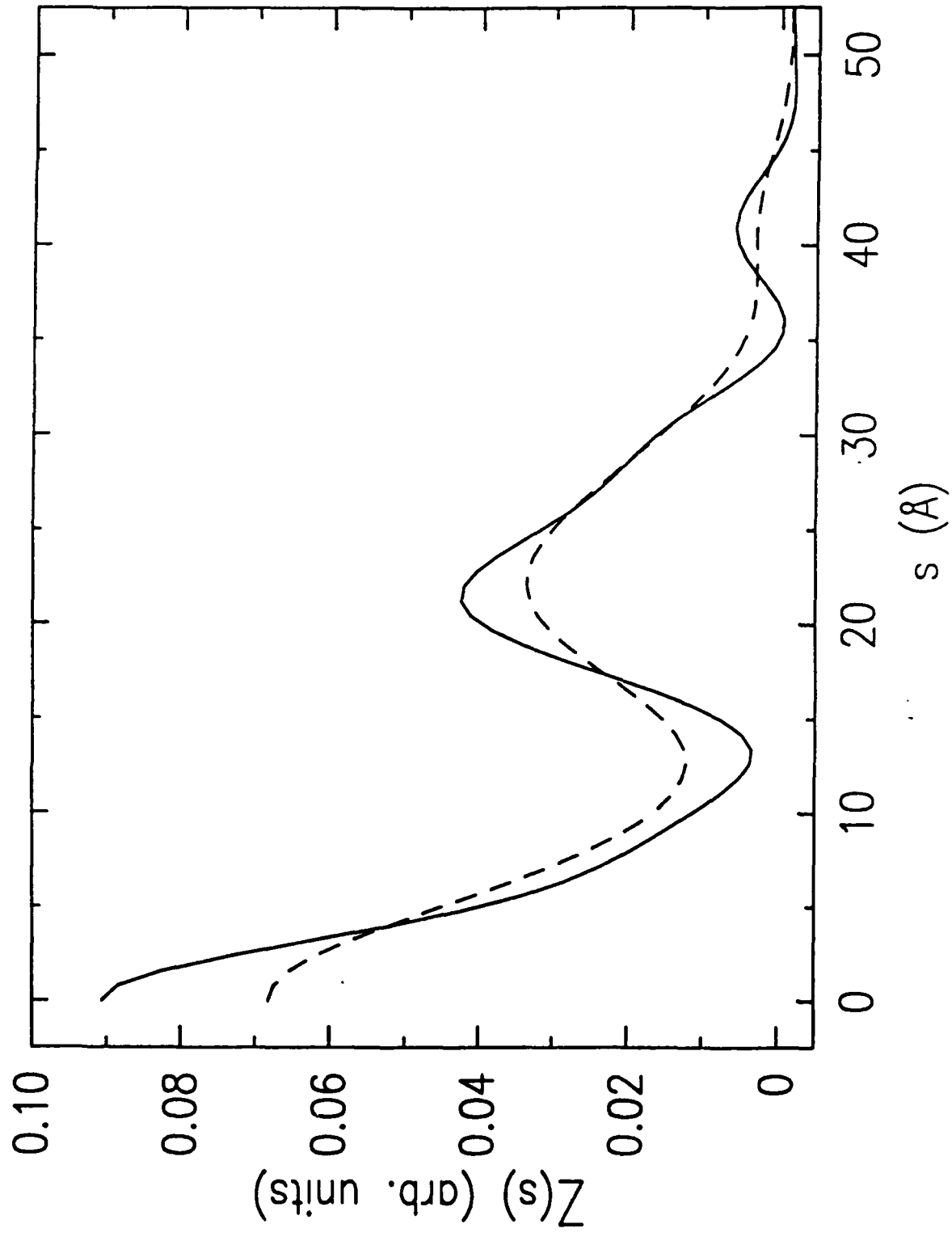

Fig. 6
Tidswell et

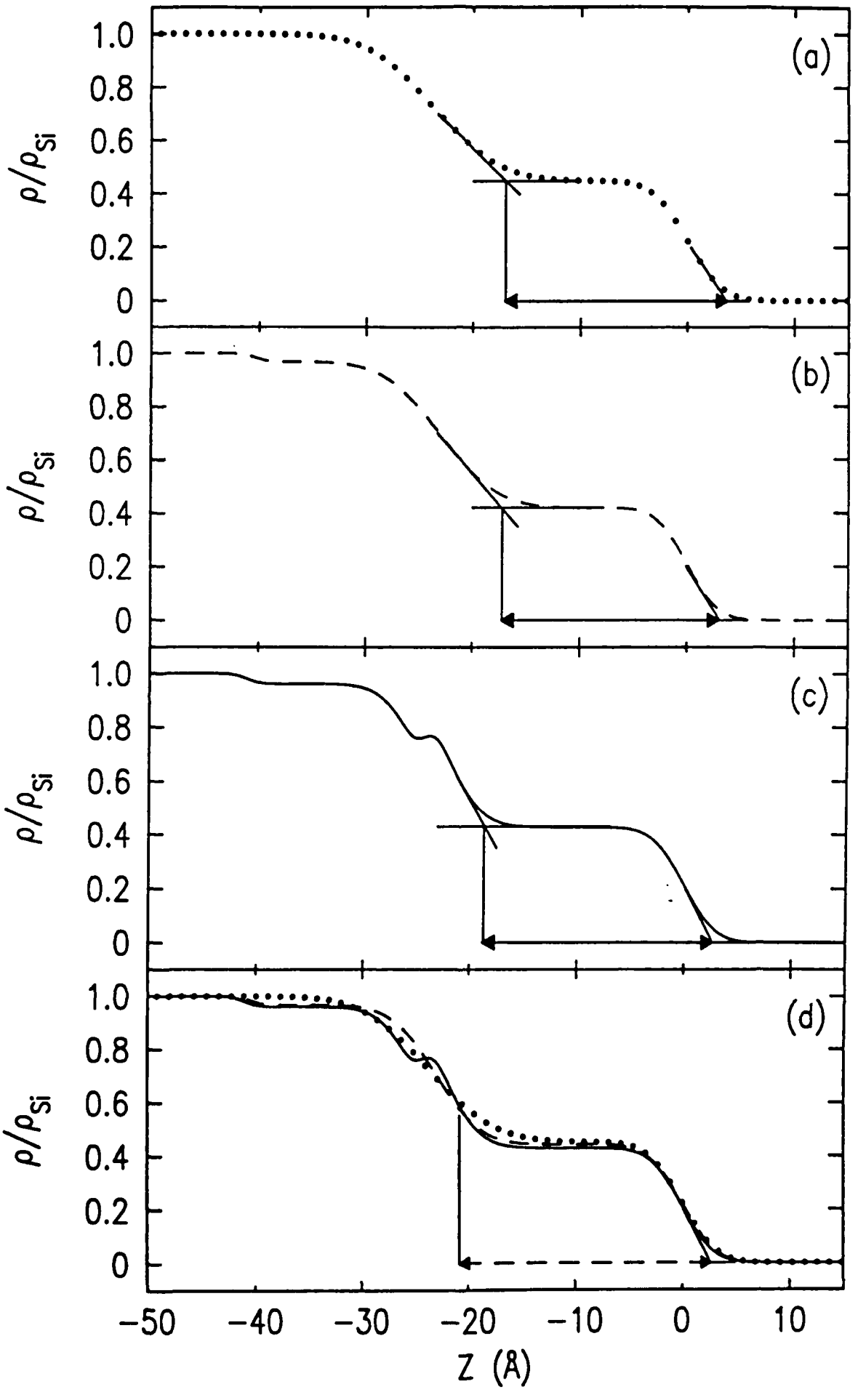

Fig. 7
Tidswell et c

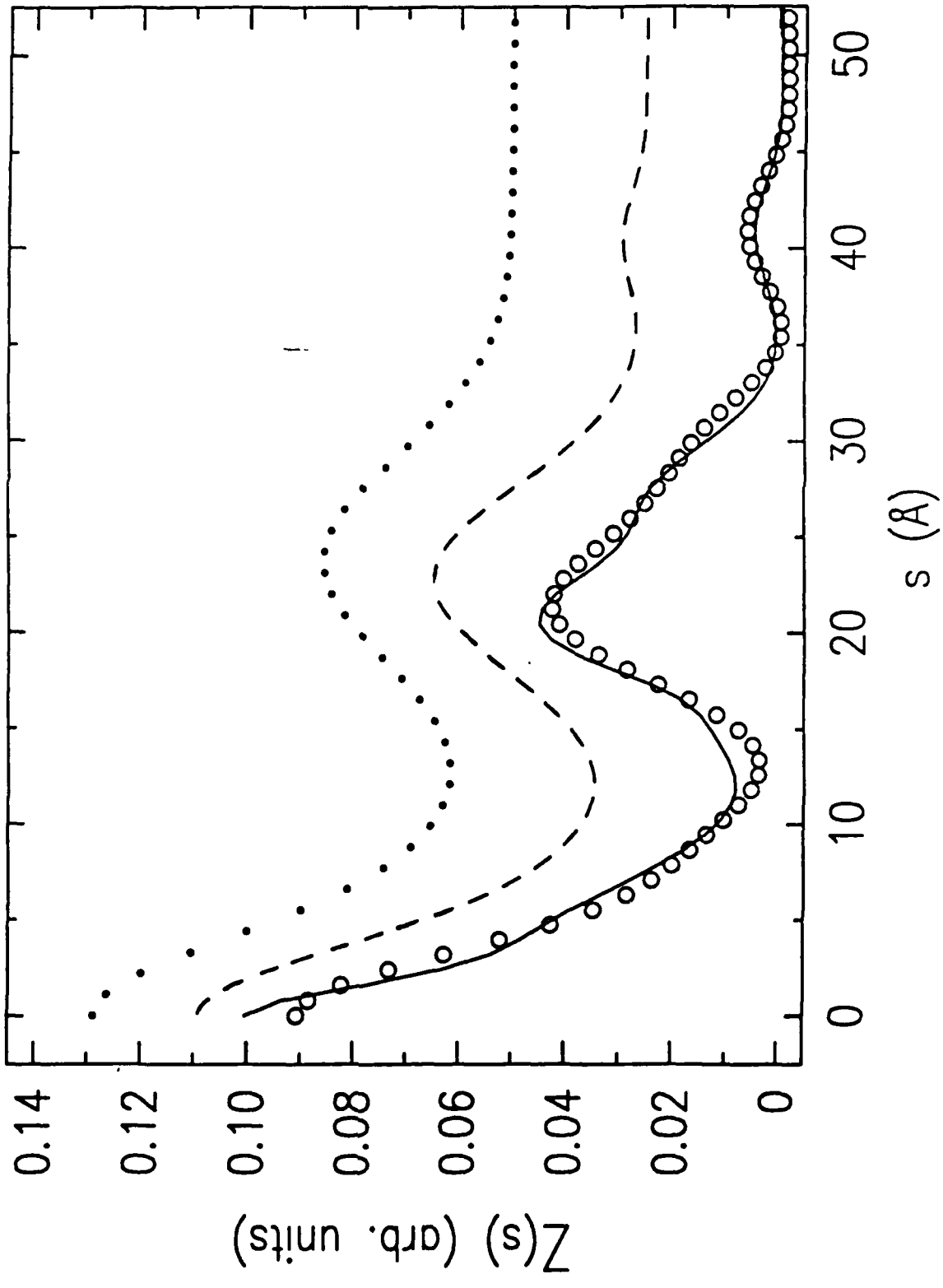

Fig. 8
Tidswell et

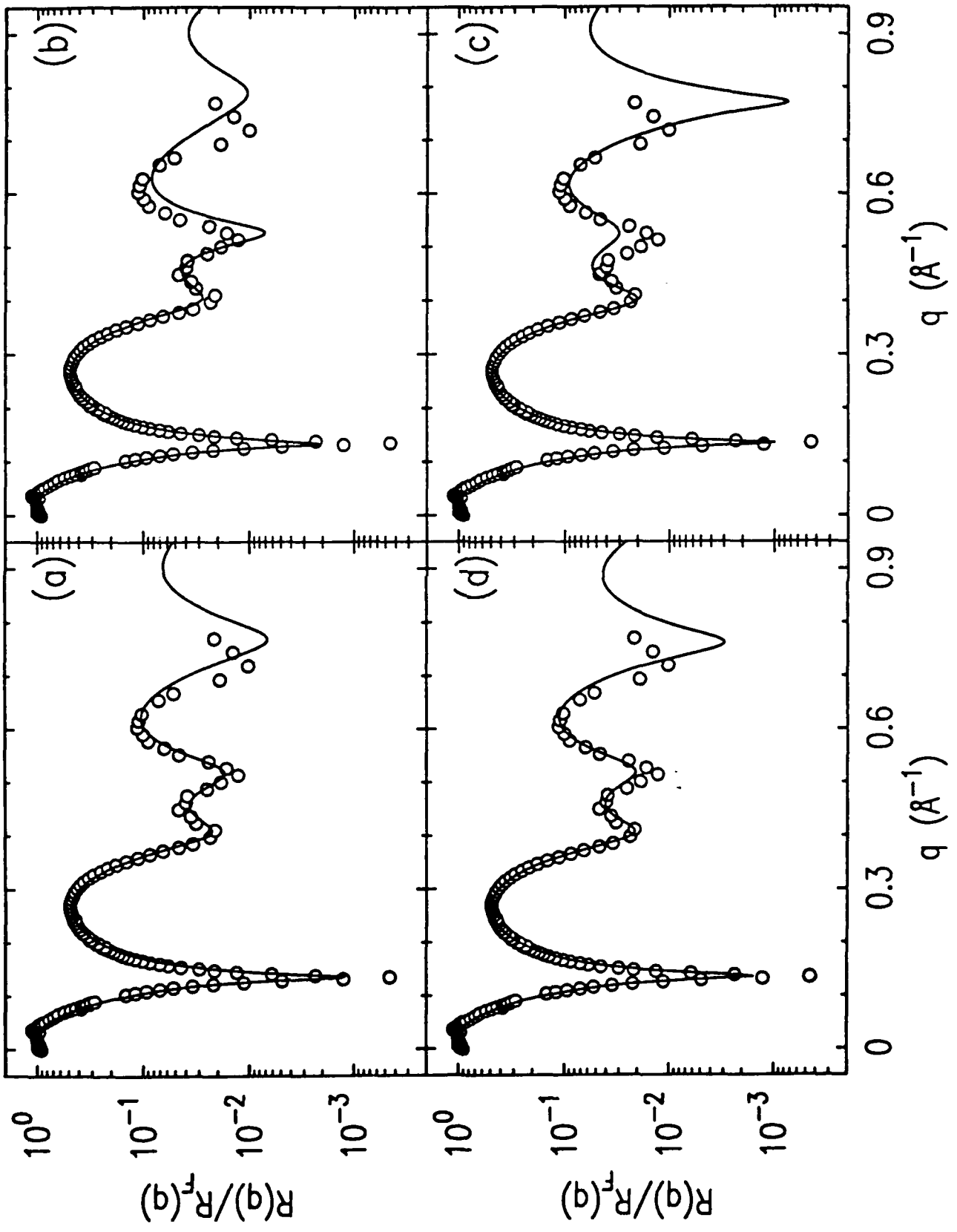

Fig. 9
Tidswell et

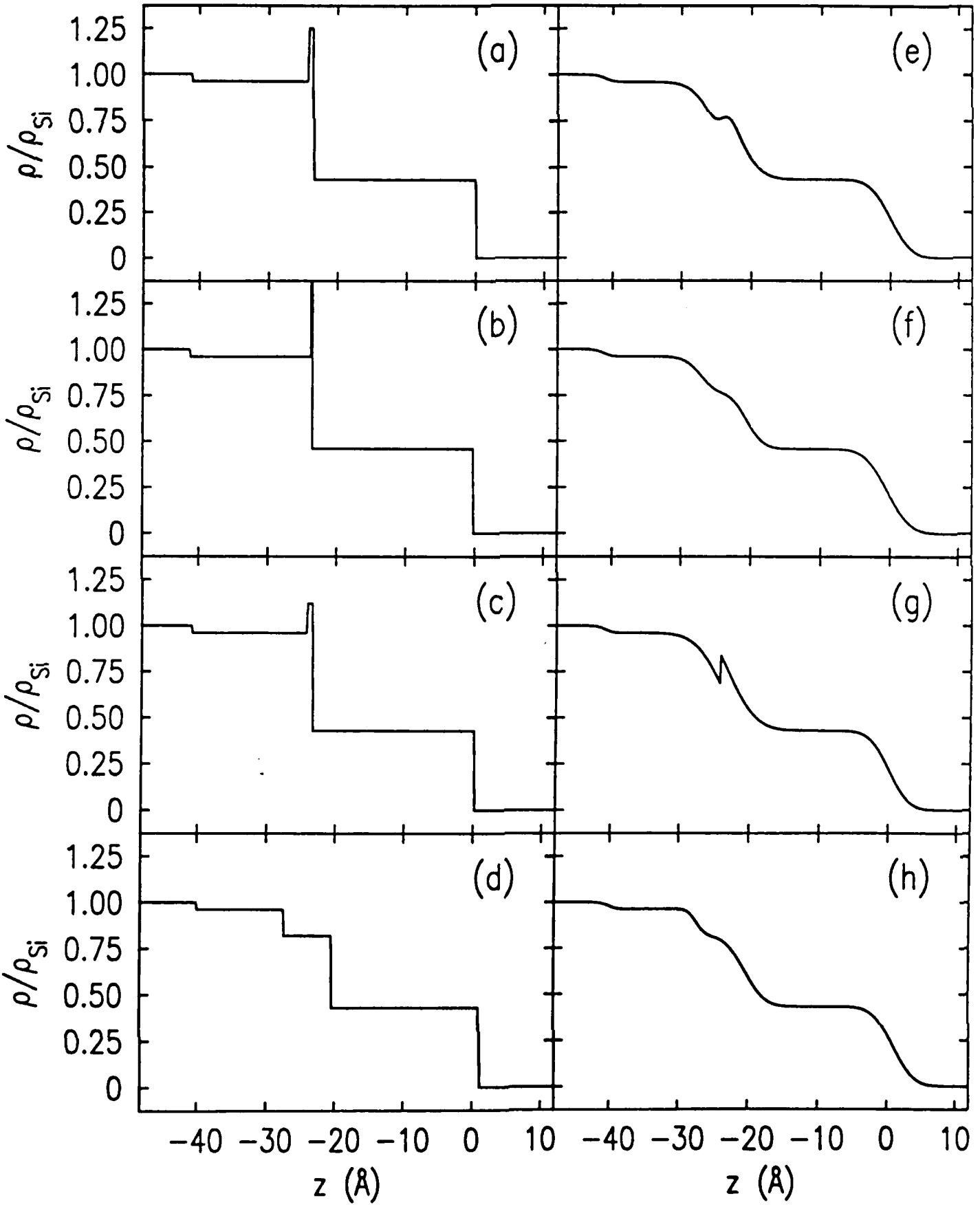

Fig. 9i
Tidswell et al.

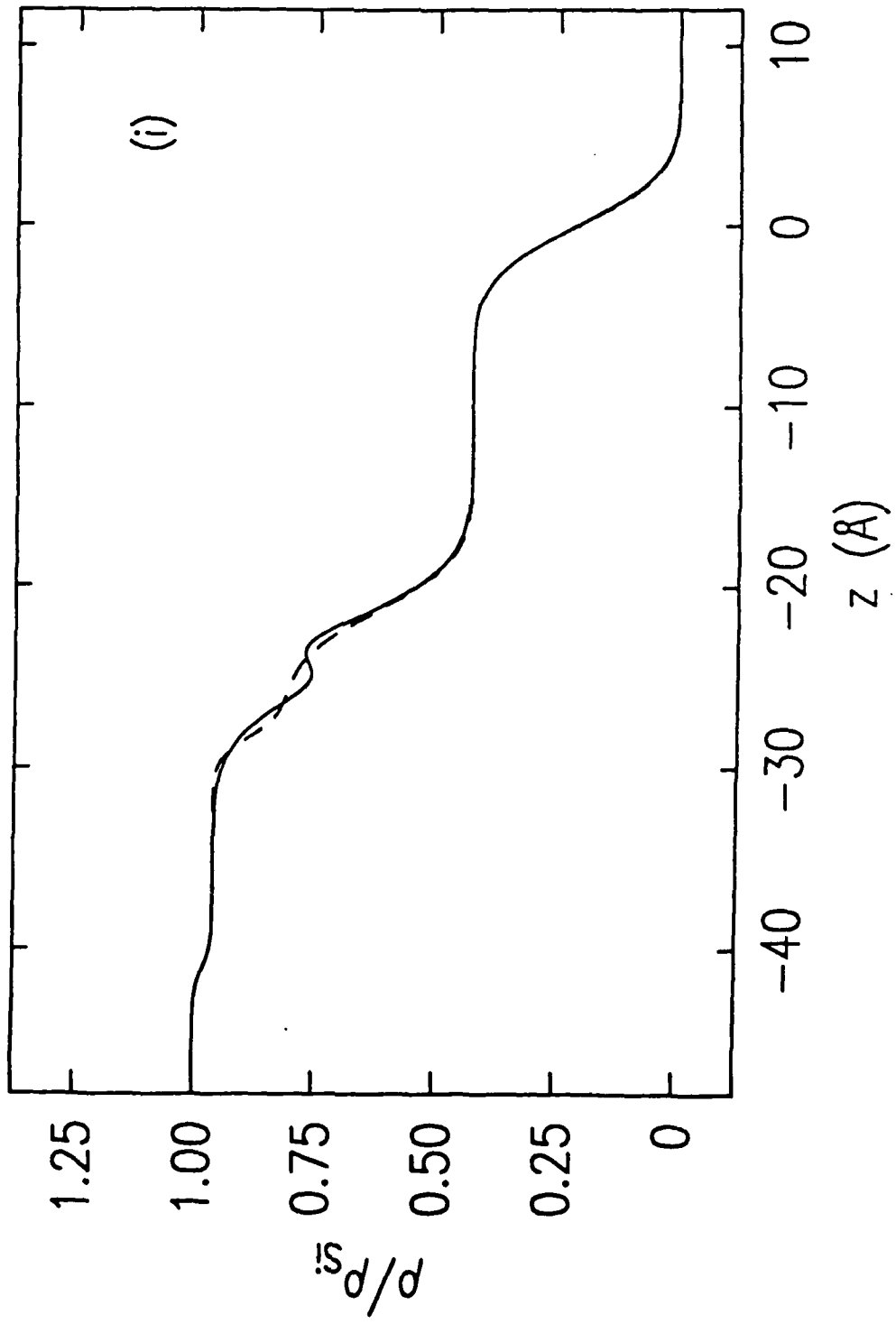

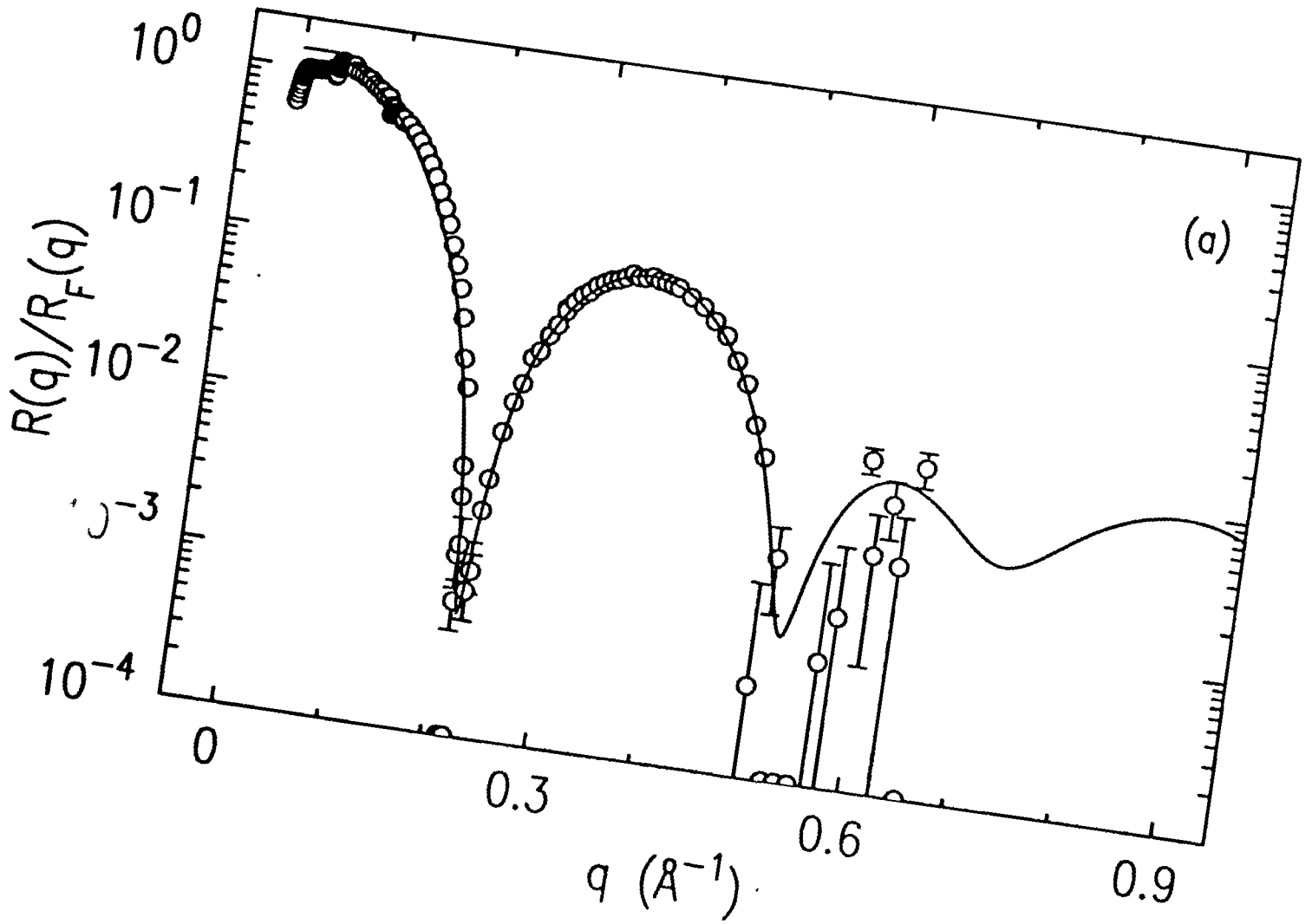

Fig. 10a
Tidswell et al

Fig. 10b
Tidswell et

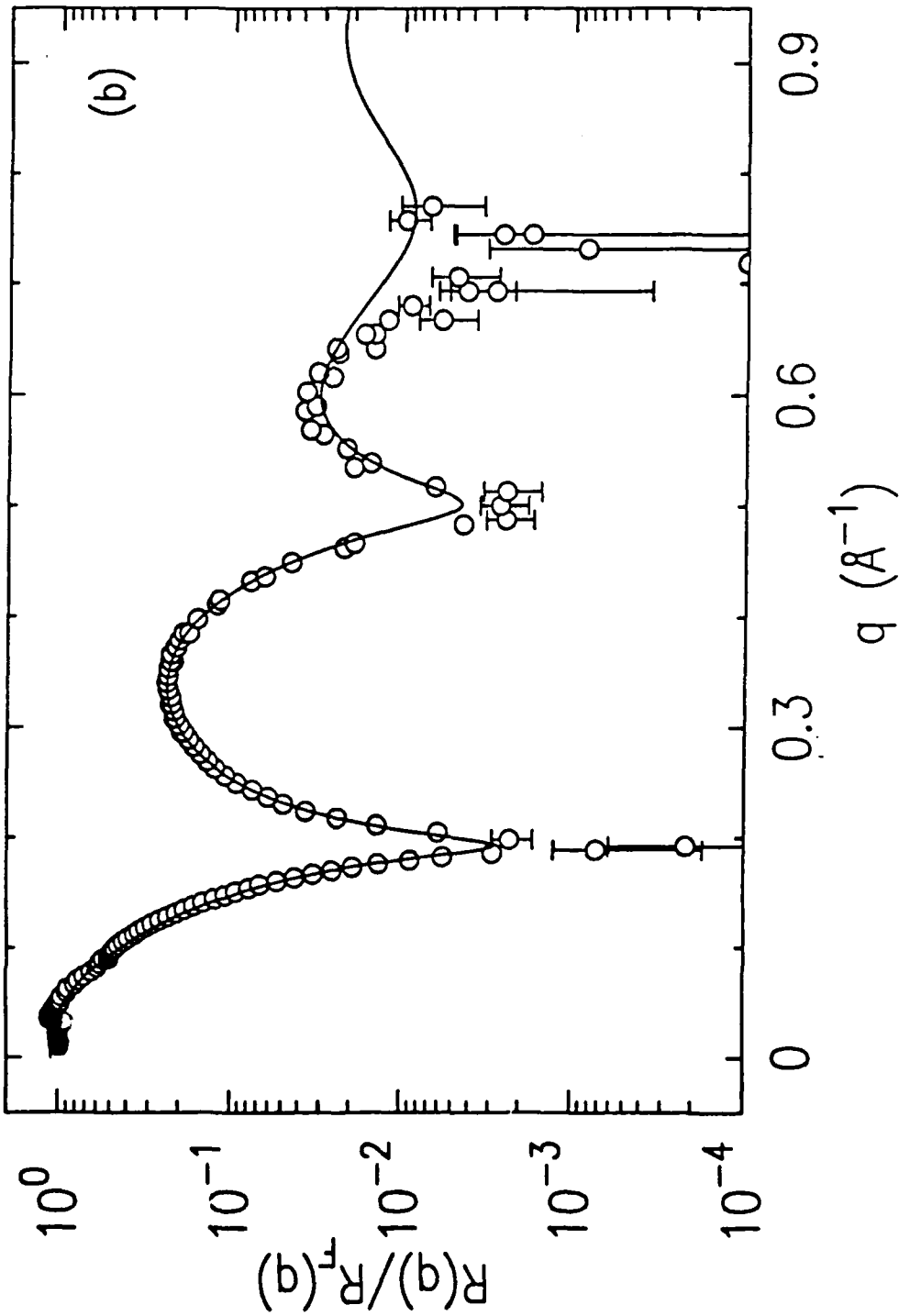

Fig. 11
Tidswell et a

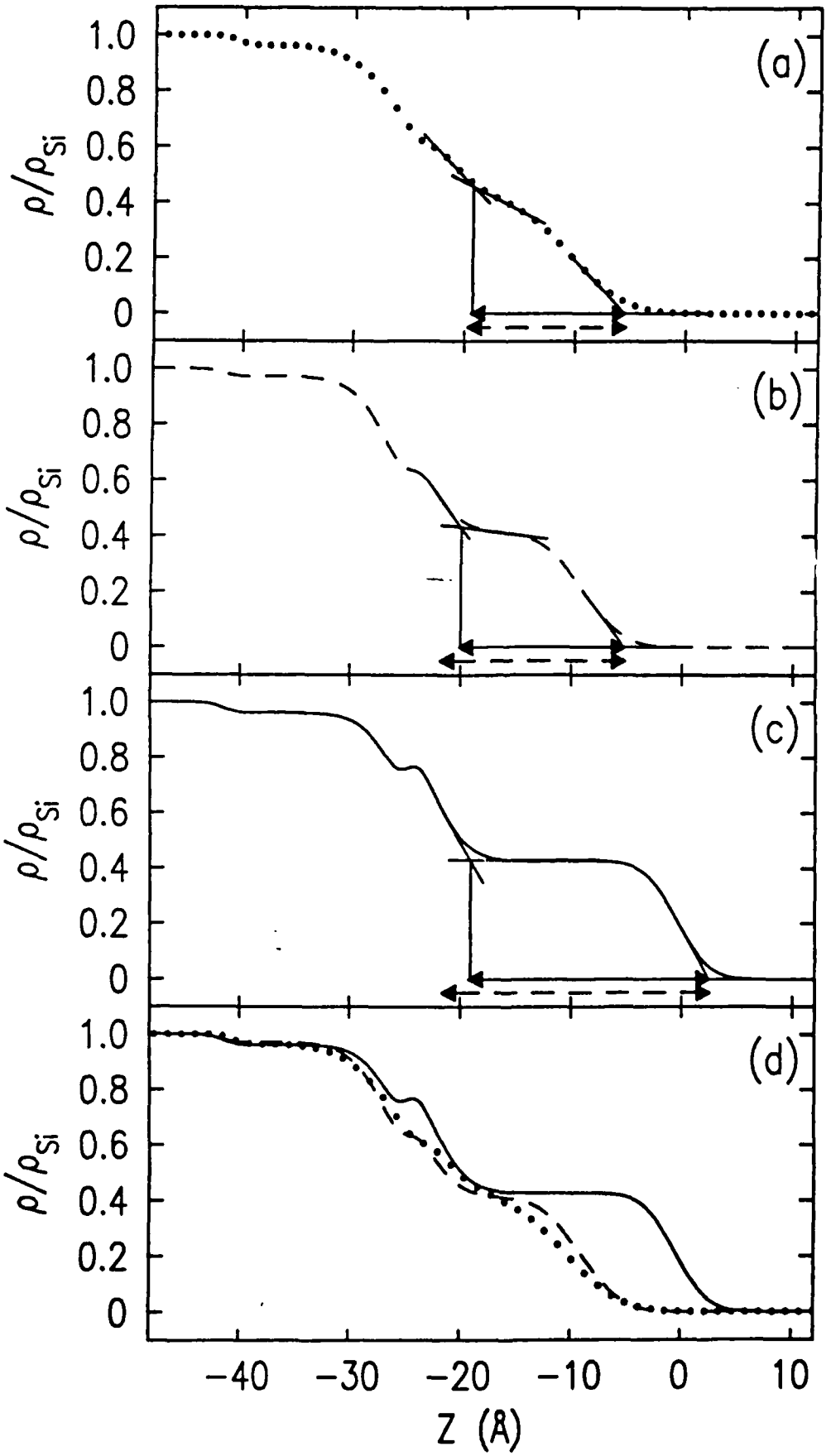

Fig. 12
Tidswell et al.

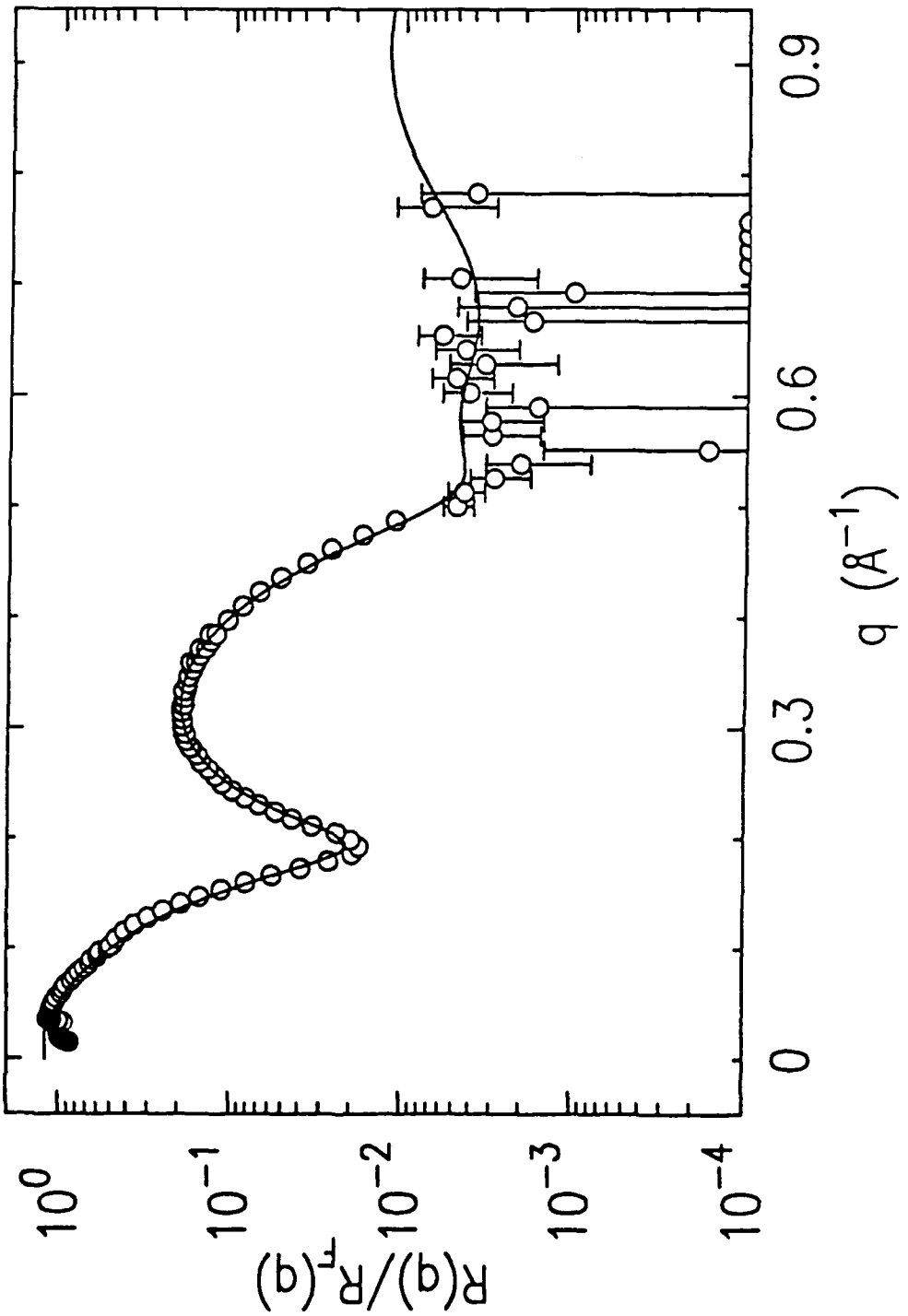

Fig. 13
Tidswell et al

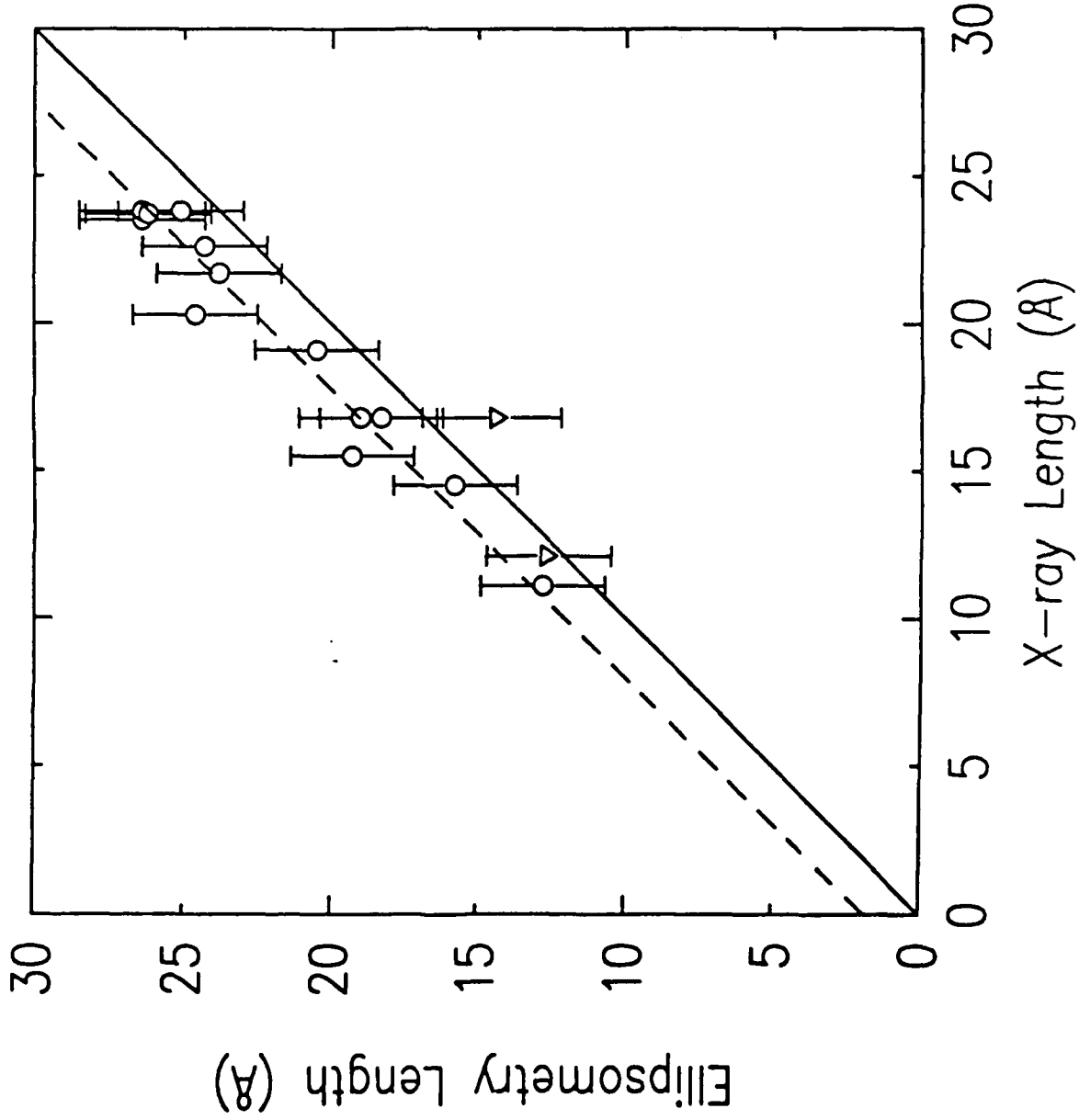

Fig. 14
Tidswell et al.

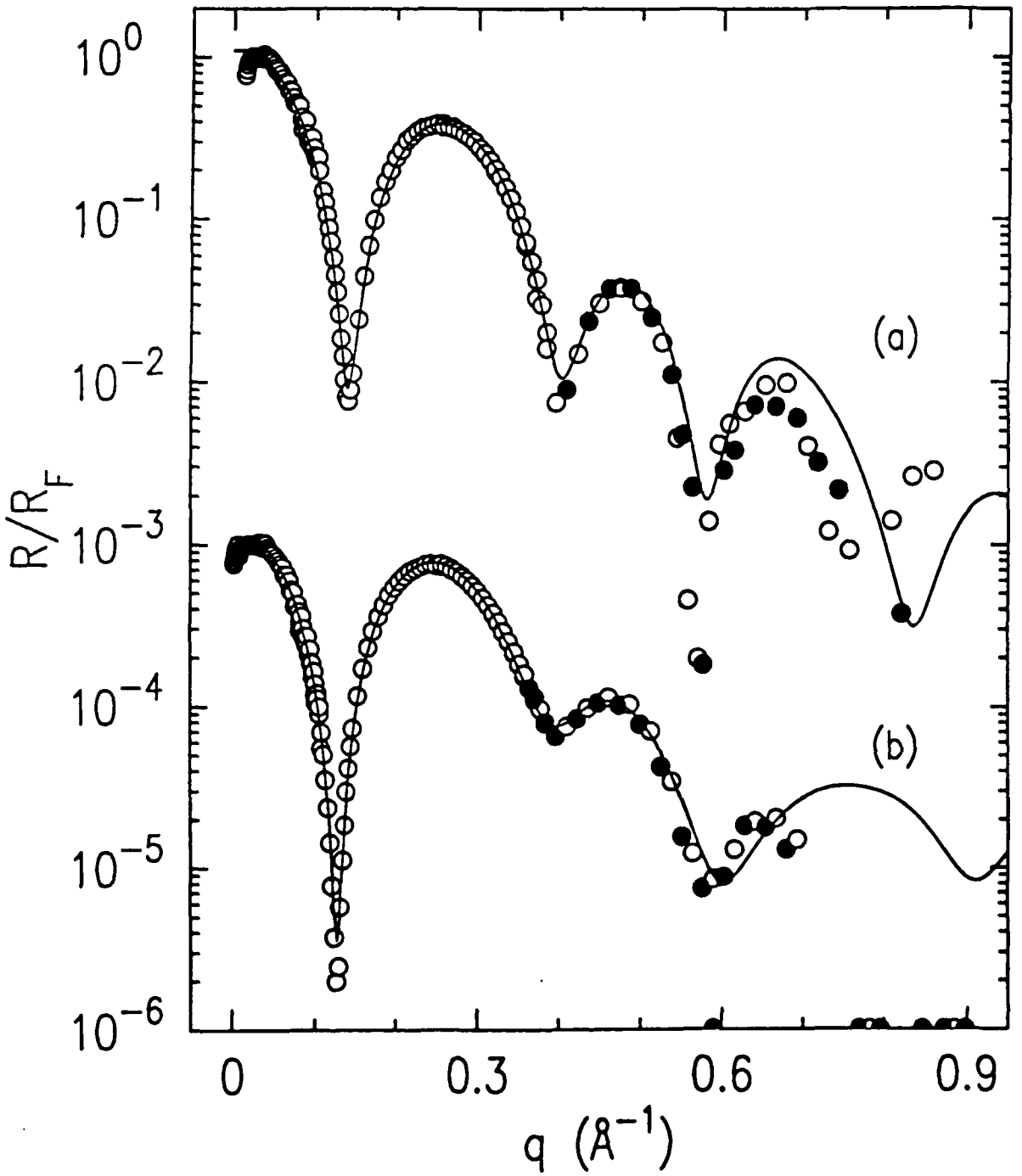

Fig. 15
Tidswell et al.

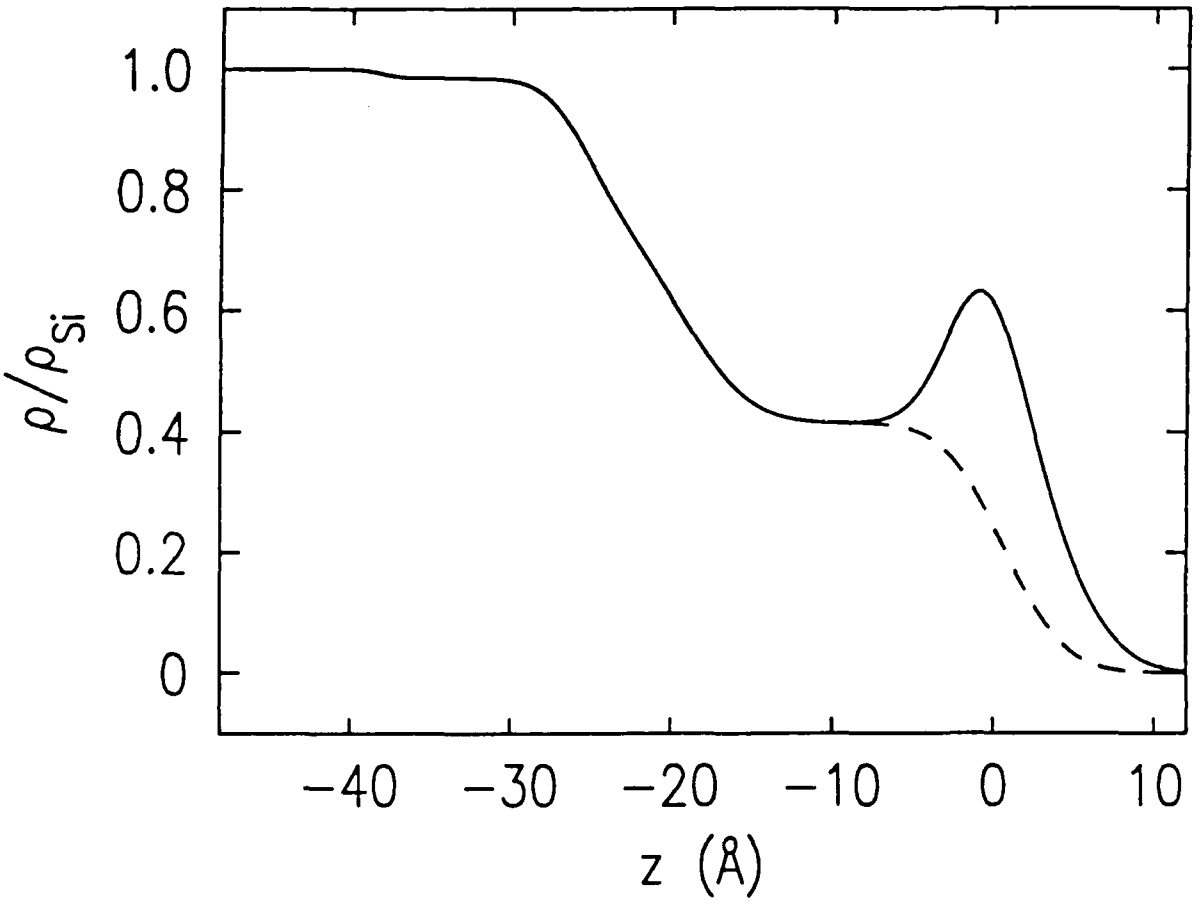

Fig. 16a
Tidswell et al.

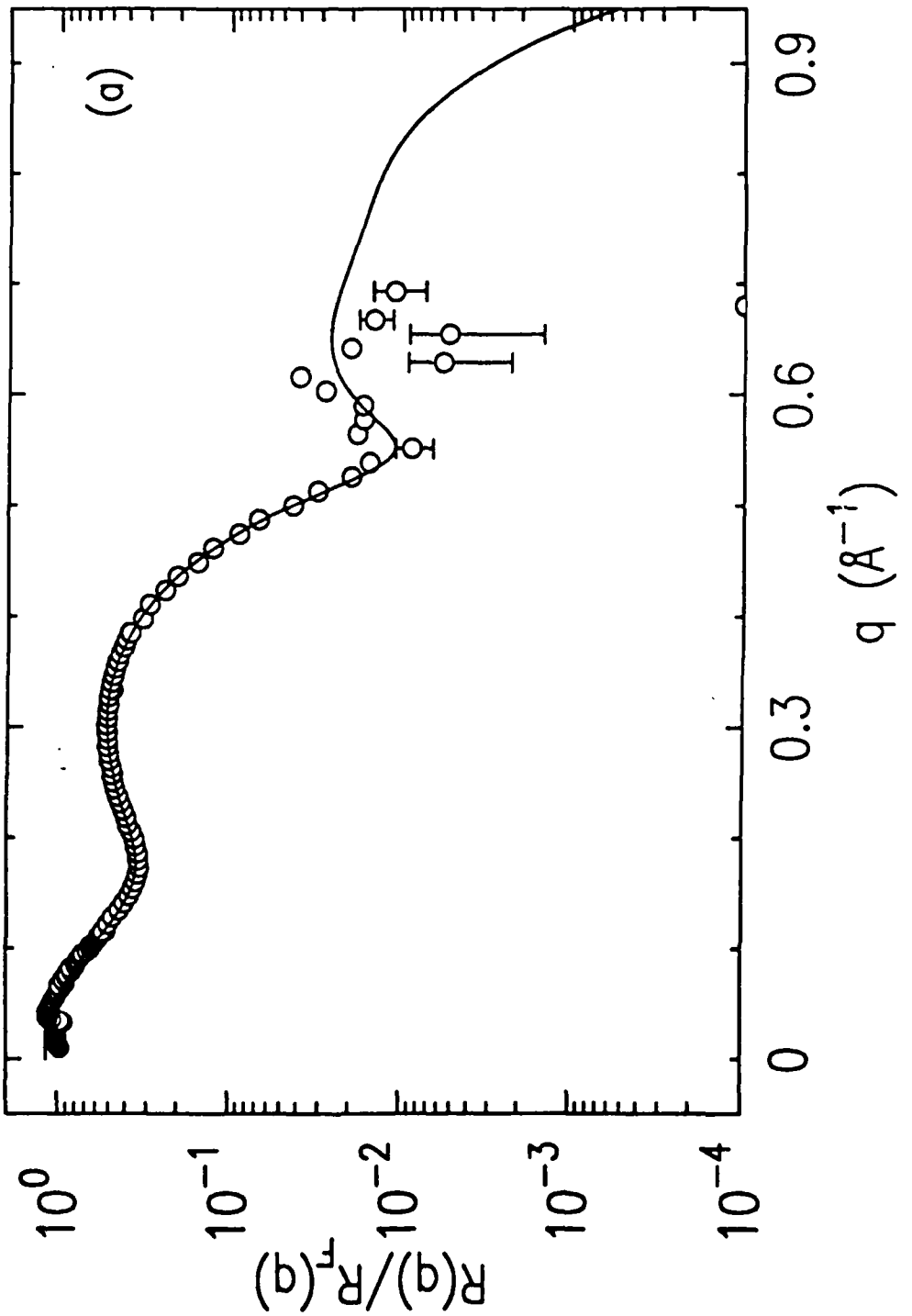

Fig. 16b
Tidswell et a

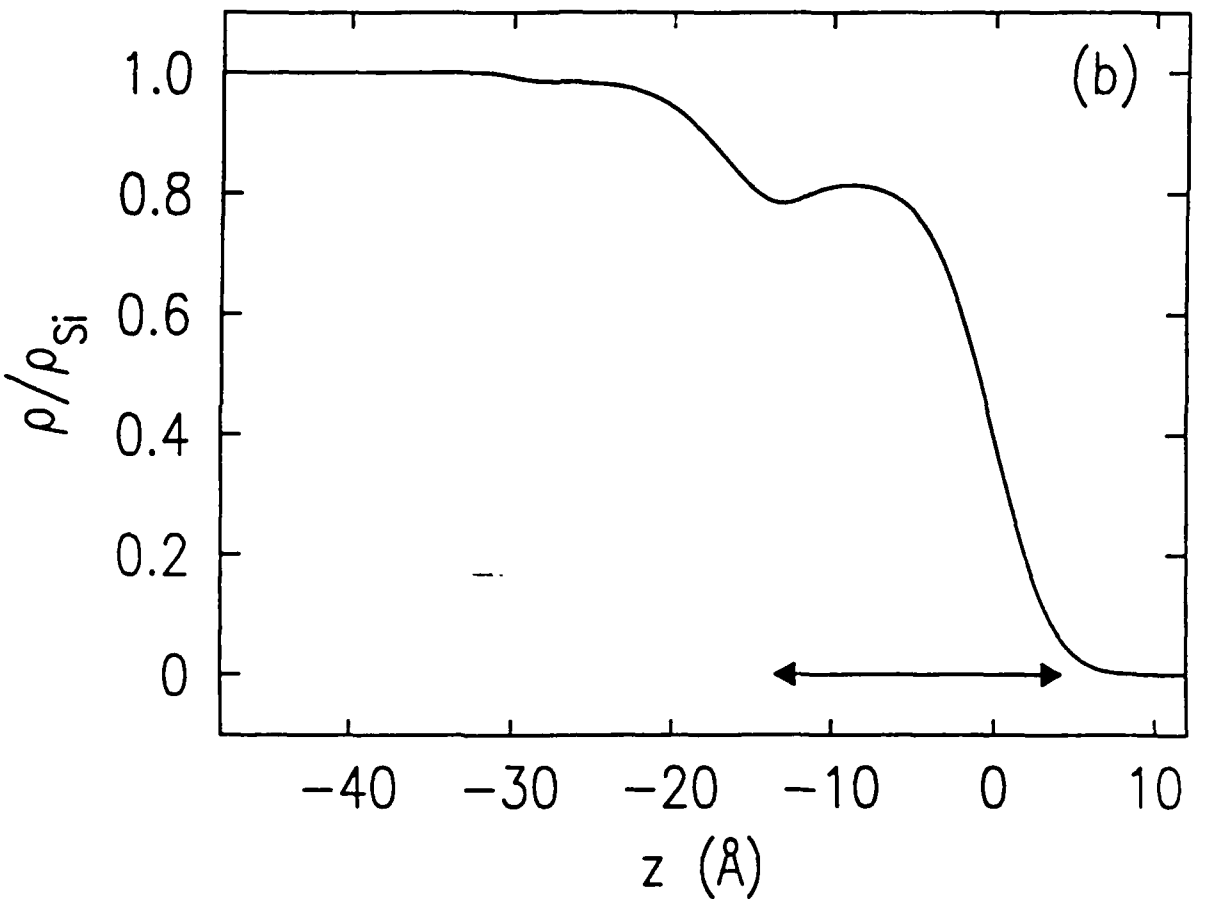

DL/1113/89/1

TECHNICAL REPORT DISTRIBUTION LIST, GENERAL

	No. Copies
Office of Naval Research Chemistry Division, Code 1113 800 North Quincy Street Arlington, VA 22217-5000	3
Commanding Officer Naval Weapons Support Center Attn: Dr. Bernard E. Douda Crane, IN 47522-5050	1
Dr. Richard W. Drisko Naval Civil Engineering Laboratory Code L52 Port Hueneme, California 93043	1
Defense Technical Information Center Building 5, Cameron Station Alexandria, Virginia 22314	2 high quality
David Taylor Research Center Dr. Eugene C. Fischer Annapolis, MD 21402-5067	1
Dr. James S. Murday Chemistry Division, Code 6100 Naval Research Laboratory Washington, D.C. 20375-5000	1
Dr. Ronald L. Atkins Chemistry Division (Code 385) Naval Weapons Center China Lake, CA 93555-6001	1
Chief of Naval Research Special Assistant for Marine Corps Matters Code 00MC 800 North Quincy Street Arlington, VA 22217-5000	1
Dr. Bernadette Eichinger Naval Ship Systems Engineering Station Code 053 Philadelphia Naval Base Philadelphia, PA 19112	1
Dr. Sachio Yamamoto Naval Ocean Systems Center Code 52 San Diego, CA 92152-5000	1
David Taylor Research Center Dr. Harold H. Singerman Annapolis, MD 21402-5067 ATTN: Code 283	1

ORGANIC CHEMISTRY & MOLECULAR RECOGNITION - Distribution List

Professor Robert W. Armstrong
Department of Chemistry
University of California
405 Hilgard Avenue
Los Angeles, CA 90024
R&T Code 4135020

Professor Bruce D. Beaver
Department of Chemistry
Duquesne University
Pittsburgh, PA 15282
R&T Code 4135016

Professor Jerald S. Bradshaw
Department of Chemistry
Brigham Young University
Provo, UT 84602
R&T Code 413p002

Professor Ronald Breslow
Department of Chemistry
Columbia University
New York, NY 10027
R&T Code 413p005

Professor Cynthia J. Burrows
Department of Chemistry
State University of New York
at Stony Brook
Stony Brook, NY 11794-3400
R&T Code 413p009

Professor Anthony W. Czarnik
Department of Chemistry
Ohio State University
120 West 18th Avenue
Columbus, OH 43210-1173
R&T Code 413p002

Professor Peter Dervan
Department of Chemistry
California Institute of Technology
Pasadena, CA 91125
R&T Code 4135018

Professor Francois N. Diederich
Department of Chemistry
University of California
405 Hilgard Avenue
Los Angeles, CA 90024
R&T Code 413b012

Professor Dennis A. Dougherty
Department of Chemistry
California Institute of Technology
Pasadena, CA 91125
R&T Code 413p006

Professor Kenneth M. Doxsee
Department of Chemistry
University of Southern California
Los Angeles, CA 90089-1062
R&T Code 413p001

Professor Margaret C. Etter
Department of Chemistry
University of Minnesota
207 Pleasant Street, S.E.
Minneapolis, MN 55455
R&T Code 4135010

Professor Wilmer K. Fife
Department of Chemistry
Indiana University-Purdue University
at Indianapolis
1125 East 38th Street
P.O. Box 647
Indianapolis, IN 46223
R&T Code 4135021

Dr. Richard Hollins
Naval Weapons Center
Chemistry Division
Research Department
China Lake, CA 93555
R&T Code 413b002

Professor Thomas J. McCarthy
Department of Polymer Science
University of Massachusetts
Room 701 Graduate Research Center
Amherst, MA 01003
R&T Code 400x015

Professor Arthur E. Martell
Department of Chemistry
Texas A&M University
College Station, TX 77843-3255
R&T Code 4135017

Professor William L. Mock
Department of Chemistry
University of Illinois at Chicago
Chicago, IL 60680
R&T Code 413p004

Professor Martin E. Newcomb
Department of Chemistry
Texas A&M University
Box 3578
College Station, TX 77843-3255
R&T Code 4135009

Professor Peter Schultz
Department of Chemistry
University of California
Berkeley, CA 94720
R&T Code 413j005

Professor Carol Venanzi
Department of Chemistry
New Jersey Institute of Technology
323 King Blvd.
Newark, NJ 07102
R&T Code 413p008

Professor George M. Whitesides
Department of Chemistry
Harvard College
Cambridge, MA 02138
R&T Code a400011dd2

Professor Howard W. Whitlock
Department of Chemistry
University of Wisconsin
Madison, WI 53706
R&T Code 413p007

Professor Jeffrey D. Winkler
Department of Chemistry
The University of Chicago
5735 S. Ellis Avenue
Chicago, IL 60637
R&T Code 413b013